EUROPEAN ORGANISATION FOR PARTICLE PHYSICS

CERN-PPE/93-46
9 March 1993

Measurement of $\Gamma(Z^0 \to b\bar{b})/\Gamma(Z^0 \to \text{hadrons})$ using Leptons

The OPAL Collaboration

Abstract

The fraction of $b\bar{b}$ events in hadronic Z^0 decays has been measured from the yield of leptons in the data samples collected by OPAL in 1990 and 1991. A sample enriched in events containing $Z^0 \to b\bar{b}$ decays was obtained by requiring the presence of an electron or muon with high momentum and high momentum component transverse to the associated hadronic jet. After accounting for backgrounds and acceptances, a value of

$$\frac{\Gamma(Z^0 \to b\bar{b})}{\Gamma(Z^0 \to \text{hadrons})} = 0.220 \pm 0.002 \pm 0.006 \pm 0.011$$

was obtained. The first two errors reflect the data statistics and the systematic uncertainties arising from detector modelling uncertainties, respectively. The third error includes systematic effects from b and c fragmentation and decay uncertainties.

(Submitted to Zeitschrift für Physik C)

The OPAL Collaboration

P.D. Acton[25], G. Alexander[23], J. Allison[16], P.P. Allport[5], K.J. Anderson[9], S. Arcelli[2], A. Astbury[28], D. Axen[29], G. Azuelos[18,a], G.A. Bahan[16], J.T.M. Baines[16], A.H. Ball[17], J. Banks[16], R.J. Barlow[16], S. Barnett[16], J.R. Batley[5], G. Beaudoin[18], A. Beck[23], G.A. Beck[13], J. Becker[10], T. Behnke[27], K.W. Bell[20], G. Bella[23], P. Bentkowski[18], P. Berlich[10], S. Bethke[11], O. Biebel[3], U. Binder[10], I.J. Bloodworth[1], P. Bock[11], B. Boden[3], H.M. Bosch[11], H. Breuker[8], P. Bright-Thomas[25], R.M. Brown[20], A. Buijs[8], H.J. Burckhart[8], C. Burgard[27], P. Capiluppi[2], R.K. Carnegie[6], A.A. Carter[13], J.R. Carter[5], C.Y. Chang[17], D.G. Charlton[8], S.L. Chu[4], P.E.L. Clarke[25], I. Cohen[23], J.C. Clayton[1], W.J. Collins[5], J.E. Conboy[15], M. Cooper[22], M. Coupland[14], M. Cuffiani[2], S. Dado[22], G.M. Dallavalle[2], S. De Jong[13], L.A. del Pozo[5], H. Deng[17], A. Dieckmann[11], M. Dittmar[4], M.S. Dixit[7], E. do Couto e Silva[12], J.E. Duboscq[8], E. Duchovni[26], G. Duckeck[11], I.P. Duerdoth[16], D.J.P. Dumas[6], P.A. Elcombe[5], P.G. Estabrooks[6], E. Etzion[23], H.G. Evans[9], F. Fabbri[2], M. Fierro[2], M. Fincke-Keeler[28], H.M. Fischer[3], D.G. Fong[17], M. Foucher[17], A. Gaidot[21], O. Ganel[26], J.W. Gary[4], J. Gascon[18], R.F. McGowan[16], N.I. Geddes[20], C. Geich-Gimbel[3], S.W. Gensler[9], F.X. Gentit[21], G. Giacomelli[2], R. Giacomelli[2], V. Gibson[5], W.R. Gibson[13], J.D. Gillies[20], J. Goldberg[22], M.J. Goodrick[5], W. Gorn[4], C. Grandi[2], F.C. Grant[5], J. Hagemann[27], G.G. Hanson[12], M. Hansroul[8], C.K. Hargrove[7], P.F. Harrison[13], J. Hart[8], P.M. Hattersley[1], M. Hauschild[8], C.M. Hawkes[8], E. Heflin[4], R.J. Hemingway[6], R.D. Heuer[8], J.C. Hill[5], S.J. Hillier[8], T. Hilse[10], D.A. Hinshaw[18], J.D. Hobbs[8], P.R. Hobson[25], D. Hochman[26], R.J. Homer[1], A.K. Honma[28,a], R.E. Hughes-Jones[16], R. Humbert[10], P. Igo-Kemenes[11], H. Ihssen[11], D.C. Imrie[25], A.C. Janissen[6], A. Jawahery[17], P.W. Jeffreys[20], H. Jeremie[18], M. Jimack[2], M. Jobes[1], R.W.L. Jones[13], P. Jovanovic[1], C. Jui[4], D. Karlen[6], K. Kawagoe[24], T. Kawamoto[24], R.K. Keeler[28], R.G. Kellogg[17], B.W. Kennedy[15], S. Kluth[5], T. Kobayashi[24], D.S. Koetke[8], T.P. Kokott[3], S. Komamiya[24], L. Köpke[8], J.F. Kral[8], R. Kowalewski[6], J. von Krogh[11], J. Kroll[9], M. Kuwano[24], P. Kyberd[13], G.D. Lafferty[16], R. Lahmann[17], F. Lamarche[18], J.G. Layter[4], P. Leblanc[18], A.M. Lee[17], M.H. Lehto[15], D. Lellouch[26], C. Leroy[18], J. Letts[4], S. Levegrün[3], L. Levinson[26], S.L. Lloyd[13], F.K. Loebinger[16], J.M. Lorah[17], B. Lorazo[18], M.J. Losty[7], X.C. Lou[12], J. Ludwig[10], M. Mannelli[8], S. Marcellini[2], G. Maringer[3], C. Markus[3], A.J. Martin[13], J.P. Martin[18], T. Mashimo[24], P. Mättig[3], U. Maur[3], J. McKenna[28], T.J. McMahon[1], J.R. McNutt[25], F. Meijers[8], D. Menszner[11], F.S. Merritt[9], H. Mes[7], A. Michelini[8], R.P. Middleton[20], G. Mikenberg[26], J. Mildenberger[6], D.J. Miller[15], R. Mir[12], W. Mohr[10], C. Moisan[18], A. Montanari[2], T. Mori[24], M. Morii[24], T. Mouthuy[12,b], B. Nellen[3], H.H. Nguyen[9], M. Nozaki[24], S.W. O'Neale[1], F.G. Oakham[7], F. Odorici[2], H.O. Ogren[12], C.J. Oram[28,a], M.J. Oreglia[9], S. Orito[24], J.P. Pansart[21], B. Panzer-Steindel[8], P. Paschievici[26], G.N. Patrick[20], N. Paz-Jaoshvili[23], P. Pfister[10], J.E. Pilcher[9], J. Pinfold[31], D. Pitman[28], D.E. Plane[8], P. Poffenberger[28], B. Poli[2], A. Pouladdej[6], T.W. Pritchard[13], H. Przysiezniak[18], G. Quast[27], M.W. Redmond[9], D.L. Rees[8], G.E. Richards[16], D. Robinson[8], A. Rollnik[3], J.M. Roney[28,c], E. Ros[8], S. Rossberg[10], A.M. Rossi[2], M. Rosvick[28], P. Routenburg[6], K. Runge[10], O. Runolfsson[8], D.R. Rust[12], M. Sasaki[24], C. Sbarra[8], A.D. Schaile[10], O. Schaile[10], W. Schappert[6], P. Scharff-Hansen[8], P. Schenk[4], B. Schmitt[3], H. von der Schmitt[11], S. Schreiber[3], C. Schwick[27], J. Schwiening[3], W.G. Scott[20], M. Settles[12], T.G. Shears[5], B.C. Shen[4], C.H. Shepherd-Themistocleous[7], P. Sherwood[15], R. Shypit[29], A. Simon[3], P. Singh[13], G.P. Siroli[2], A. Skuja[17], A.M. Smith[8], T.J. Smith[28], G.A. Snow[17], R. Sobie[28,c], R.W. Springer[17], M. Sproston[20], K. Stephens[16], J. Steuerer[28], R. Ströhmer[11], D. Strom[30], T. Takeshita[24,d], P. Taras[18], S. Tarem[26], M. Tecchio[9], P. Teixeira-Dias[11], N. Tesch[3], N.J. Thackray[1], M.A. Thomson[15], E. Torrente-Lujan[22], G. Transtromer[25], N.J. Tresilian[16], T. Tsukamoto[24], M.F. Turner[8], G. Tysarczyk-Niemeyer[11], D. Van den plas[18], R. Van Kooten[27], G.J. VanDalen[4], G. Vasseur[21], C.J. Virtue[7], A. Wagner[27], D.L. Wagner[9], C. Wahl[10], J.P. Walker[1], C.P. Ward[5], D.R. Ward[5], P.M. Watkins[1], A.T. Watson[1], N.K. Watson[8], M. Weber[11], P. Weber[6], P.S. Wells[8], N. Wermes[3], M.A. Whalley[1], G.W. Wilson[4], J.A. Wilson[1], V-H. Winterer[10], T. Wlodek[26], S. Wotton[11], T.R. Wyatt[16], R. Yaari[26], A. Yeaman[13], G. Yekutieli[26], M. Yurko[18], W. Zeuner[8], G.T. Zorn[17].

[1]School of Physics and Space Research, University of Birmingham, Birmingham, B15 2TT, UK
[2]Dipartimento di Fisica dell' Università di Bologna and INFN, Bologna, 40126, Italy
[3]Physikalisches Institut, Universität Bonn, D-5300 Bonn 1, FRG
[4]Department of Physics, University of California, Riverside, CA 92521 USA
[5]Cavendish Laboratory, Cambridge, CB3 0HE, UK
[6]Carleton University, Dept of Physics, Colonel By Drive, Ottawa, Ontario K1S 5B6, Canada
[7]Centre for Research in Particle Physics, Carleton University, Ottawa, Ontario K1S 5B6, Canada
[8]CERN, European Organisation for Particle Physics, 1211 Geneva 23, Switzerland
[9]Enrico Fermi Institute and Department of Physics, University of Chicago, Chicago Illinois 60637, USA
[10]Fakultät für Physik, Albert Ludwigs Universität, D-7800 Freiburg, FRG
[11]Physikalisches Institut, Universität Heidelberg, Heidelberg, FRG
[12]Indiana University, Dept of Physics, Swain Hall West 117, Bloomington, Indiana 47405, USA
[13]Queen Mary and Westfield College, University of London, London, E1 4NS, UK
[14]Birkbeck College, London, WC1E 7HV, UK
[15]University College London, London, WC1E 6BT, UK
[16]Department of Physics, Schuster Laboratory, The University, Manchester, M13 9PL, UK
[17]Department of Physics, University of Maryland, College Park, Maryland 20742, USA
[18]Laboratoire de Physique Nucléaire, Université de Montréal, Montréal, Quebec, H3C 3J7, Canada
[20]Rutherford Appleton Laboratory, Chilton, Didcot, Oxfordshire, OX11 0QX, UK
[21]DAPNIA/SPP, Saclay, F-91191 Gif-sur-Yvette, France
[22]Department of Physics, Technion-Israel Institute of Technology, Haifa 32000, Israel
[23]Department of Physics and Astronomy, Tel Aviv University, Tel Aviv 69978, Israel
[24]International Centre for Elementary Particle Physics and Dept of Physics, University of Tokyo, Tokyo 113, and Kobe University, Kobe 657, Japan
[25]Brunel University, Uxbridge, Middlesex, UB8 3PH UK
[26]Nuclear Physics Department, Weizmann Institute of Science, Rehovot, 76100, Israel
[27]Universität Hamburg/DESY, II Inst für Experimental Physik, 2000 Hamburg 52, Germany
[28]University of Victoria, Dept of Physics, P O Box 3055, Victoria BC V8W 3P6, Canada
[29]University of British Columbia, Dept of Physics, 6224 Agriculture Road, Vancouver BC V6T 1Z1, Canada
[30]University of Oregon, Dept of Physics, Eugene, Oregon 97403, USA
[31]University of Alberta, Dept of Physics, Edmonton AB T6G 2J1, Canada

[a]Also at TRIUMF, Vancouver, Canada V6T 2A3
[b]Now at Centre de Physique des Particules de Marseille, Faculté des Sciences de Luminy, Marseille
[c]And IPP, University of Victoria, Dept of Physics, P O Box 3055, Victoria BC V8W 3P6, Canada
[d]Also at Shinshu University, Matsumoto 390, Japan

1 Introduction

The partial decay widths of the Z^0 via the different quark and lepton channels are predicted in the Standard Model. The leptonic partial widths and the total hadronic width have been measured with about 1% precision at LEP [1] and are in good agreement with prediction. The decay widths to quarks, on the other hand, are measured with much larger errors. For b quarks, the partial decay width, $\Gamma(Z^0 \to b\overline{b})$, has been measured with typically 10% precision [2–8]. Electroweak corrections involving the top quark affect the partial decay width of the Z^0 to b quarks differently from the decay widths to lighter quarks. This results in a reduced dependence of the $Z^0 \to b\overline{b}$ decay width on the top quark mass. Precise measurements of this decay width would therefore be a way to test the Standard Model with less sensitivity to the uncertainty on the top mass [9].

Leptons with high momentum and large momentum component transverse to jets are a well established signature for b quarks. A large fraction of such leptons are expected to come from semileptonic decays of b hadrons, because of the relatively large mass and hard fragmentation of the b quark. Since at LEP essentially all b quarks produced originate from Z^0 decays, the yield of these leptons allows the fraction

$$\frac{\Gamma(Z^0 \to b\overline{b})}{\Gamma(Z^0 \to \text{hadrons})} \equiv \frac{\Gamma_{b\bar{b}}}{\Gamma_{had}}$$

to be measured. Since Γ_{had} is known precisely from the hadronic Z^0 cross-section, this provides a measurement of $\Gamma_{b\bar{b}}$. Good knowledge of the semileptonic branching ratio $B(b \to \ell)$[1] (ℓ denotes e or μ) and of the lepton momentum spectrum in the semileptonic decay is essential, and ultimately determines the precision of the $\Gamma_{b\bar{b}}/\Gamma_{had}$ measurement for this "single lepton tag" technique. These difficulties can be avoided using double tagging techniques [7], but such measurements are statistically limited at present.

This analysis used the data collected by the OPAL experiment in 1990 and 1991, considering both electrons and muons. It supersedes the previously published measurements [2,3] based on 1990 OPAL data. Various improvements in understanding the data have been made, and the treatment of systematic uncertainties improved. Measurements of the semileptonic branching ratios of b hadrons made at the $\Upsilon(4S)$ using different theoretical models of b hadron decays were treated consistently in extracting $\Gamma_{b\bar{b}}/\Gamma_{had}$. The effects of different mixes of b hadron species at LEP compared to the $\Upsilon(4S)$, and the corresponding uncertainties, were considered.

The analysis technique is described in the next section. The most important features of the OPAL detector for the analysis are described briefly in section 3. Section 4 reviews the event samples used, both from the experiment and from simulation. The electron and muon identification schemes are discussed in sections 5 and 6 respectively. Section 7 describes the treatment of heavy hadron decay model and branching ratio uncertainties. The results obtained applying the technique to data are given in section 8.

2 Analysis Method

The analysis technique consisted of counting the number of leptons and breaking this number down in terms of contributions from different sources. The fraction of leptons from b hadron decays was enhanced by requiring that identified lepton candidates pass minimum momentum and transverse momentum thresholds (the exact definition of transverse momentum employed is given in section 4). The values of these thresholds were selected to give a small total error on $\Gamma_{b\bar{b}}/\Gamma_{had}$, and differ for electrons and muons because of different backgrounds and efficiencies in the two samples. For each sample, the number of leptons expected from hadronic backgrounds was subtracted, as was the pre-

[1] A reference to a particle or reaction is intended also to refer to the corresponding antiparticle equivalent.

dicted contribution from electrons from photon conversions. The remaining prompt lepton[2] candidates are expected to arise from decays of b-flavoured and c-flavoured hadrons, with some electrons also arising from Dalitz decays of π^0 and η.

For either lepton flavour, the number of candidates, N_ℓ, resulting from this procedure can be expressed

$$N_\ell = N_\ell^{\mathrm{b}} + N_\ell^{\mathrm{c}} + N_\ell^{\mathrm{other}},$$

where N_ℓ^{b}, N_ℓ^{c} are the numbers of prompt leptons from Z^0 decays to $\mathrm{b\overline{b}}$ or $\mathrm{c\overline{c}}$ pairs respectively. N_ℓ^{other} is significant only for electrons, and includes all other sources of prompt electrons, mainly Dalitz decays. Leptons arising from heavy quark-antiquark pair creation in the fragmentation process were also included.

The number of prompt electrons or muons from $\mathrm{b\overline{b}}$ events can be written

$$N_\ell^{\mathrm{b}} = 2N_{\mathrm{had}}\frac{\Gamma_{\mathrm{b\bar{b}}}}{\Gamma_{\mathrm{had}}}\sum(B\cdot\epsilon)_{\mathrm{b}},$$

where N_{had} is the number of hadronic Z^0 decays, $\sum(B\cdot\epsilon)_{\mathrm{b}}$ represents the prompt lepton contribution from direct or indirect b hadron decay, expressed as a sum of products of branching ratios B and acceptances ϵ for the different decay chains from b hadron to electron or muon. The sum $\sum(B\cdot\epsilon)_{\mathrm{b}}$ is so written because the different decay chains from b hadron to lepton have different branching ratios and acceptances, with different, but correlated, uncertainties. The acceptances ϵ include kinematic and geometrical efficiencies for each decay mode as well as the efficiency for a Z^0 decay to $\mathrm{b\overline{b}}$ to pass the hadronic event selection cuts.

The division by decay mode in the sum $\sum(B\cdot\epsilon)_{\mathrm{b}}$ is made as follows:

- The direct semileptonic decay of a hadron containing a b quark to products including an electron or muon ($\mathrm{b}\to\ell$).
- The cascade decay of a b hadron to a c hadron, which then decays semileptonically to products including an electron or muon ($\mathrm{b}\to\mathrm{c}\to\ell$). Both c quark or antiquark can be produced in the decay of a b hadron: the former from a direct decay, the latter from a virtual W.
- The production and leptonic decay of J/ψ particles from b decay ($\mathrm{b}\to\mathrm{J}/\psi\to\ell$) is considered separately, and not included in the previous category. It can be expected to be affected differently by uncertainties in modelling heavy flavour decays, since the kinematics of the two-body decay $\mathrm{J}/\psi\to\ell^+\ell^-$ should be well modelled.
- The decay of a b hadron to a τ lepton plus other products, where the τ subsequently decays to an electron or muon ($\mathrm{b}\to\tau\to\ell$).

The analysis technique of selecting only leptons with high momentum and transverse momentum results in a sample dominated by direct $\mathrm{b}\to\ell$ decays.

Analogously, the number of prompt leptons from $\mathrm{c\overline{c}}$ events can be written:

$$N_\ell^{\mathrm{c}} = 2N_{\mathrm{had}}\frac{\Gamma_{\mathrm{c\bar{c}}}}{\Gamma_{\mathrm{had}}}(B\cdot\epsilon)_{\mathrm{c}},$$

where now the product $(B\cdot\epsilon)_{\mathrm{c}}$ represents direct semileptonic decays of charm quarks ($\mathrm{c}\to\ell$) only. Leptons from direct c decays are also suppressed relative to those from direct b decays by the kinematic cuts.

[2] A "prompt" lepton is one that originates from the decay of a particle which has a lifetime of less than 10^{-11} s. Prompt leptons thus include those from decays of heavy hadrons and short-lived particles such as π^0 and η but exclude those from decays of long-lived particles such as $\mathrm{K}^\pm$ and $\pi^\pm$, and those from photon conversions to electron-positron pairs in the detector material. The division is made based on whether a decaying particle has any chance of interacting with the detector before it decays.

The measurement of $\Gamma_{b\bar{b}}/\Gamma_{had}$ by this method requires good knowledge of the different branching ratios B and acceptances ϵ. The main experimental challenge is to understand well the identification efficiencies and backgrounds for electrons and muons, as discussed in sections 5 and 6. The fragmentation of the b quark must be modelled adequately. Understanding the $b \to \ell$ decay, which is the dominant source of leptons in the final sample, is a critical issue. Detailed consideration was given to the momentum spectrum of the lepton in the decaying b hadron rest frame, and to the question of how this affects both the branching ratio measurements made at lower energies and the acceptance of this analysis. The most precise measurements of the branching ratios B have been made at lower energy experiments in $\Upsilon(4S)$ decays. The results [10] from the CLEO Collaboration were taken, because the uncertainties in the momentum spectrum were explicitly considered. Section 7 explains how these results are treated for this analysis.

3 The OPAL Detector

The OPAL detector has been described elsewhere [11], and only the components important for this analysis are reviewed. The OPAL coordinate system is defined to have its origin at the geometrical centre of the detector. The positive z axis lies along the electron beam direction and θ and ϕ are the polar and azimuthal angles. The x direction points towards the centre of the LEP ring and the y direction points upwards.

The central charged particle tracking detector is made up of a precision vertex detector, a large volume jet chamber, and thin surrounding z-chambers. The vertex detector is a high resolution drift chamber with both axial and stereo wires. In addition, a silicon microvertex detector was installed inside the vertex detector for the 1991 data-taking period. The jet chamber, approximately 4 m long and 3.7 m in diameter, provides up to 159 space points per track, and measures the ionization energy loss of charged particles [12]. It is subdivided azimuthally into 24 sectors. The central tracking chambers are maintained at a gas pressure of four atmospheres in a pressure vessel, surrounded by a solenoidal coil providing a magnetic field of 0.435 T which is uniform within the volume of the central tracking chambers. The z coordinates of jet chamber hits are determined using charge division. The precision of determination of track polar angles is improved by the z-chambers, which provide up to six measurements of the z coordinate on each track. The z-chambers cover 94% of the solid angle in the polar angle range $|\cos\theta| < 0.72$. For the combined central detector, the resolution, $\sigma(p_{xy})$, of the momentum in the bending plane of the magnetic field is given by $\sigma(p_{xy})/p_{xy} = \sqrt{(0.02)^2 + (0.0015 p_{xy})^2}$ for p_{xy} in GeV/c. The average resolution on the azimuthal track angle is 0.25 mrad. The polar angle resolution varies from 0.25 mrad for tracks with z-chamber hits to 20 mrad for tracks with only jet chamber information and constrained to the interaction point in z. The ionization energy loss measurement has a resolution of 3.5% for tracks with the maximum 159 samples.

A lead-glass electromagnetic calorimeter with a presampler surrounds the magnet coil. The calorimeter is divided into a cylindrical barrel, covering the polar angle range $|\cos\theta| < 0.82$, and annular endcaps, covering the range $0.81 < |\cos\theta| < 0.98$. The barrel calorimeter consists of 9440 lead-glass blocks arranged in a nearly projective geometry. The barrel presampler, positioned between the coil and the lead-glass, consists of two nested cylinders of limited streamer tubes covering the polar angle range $|\cos\theta| < 0.81$. In the barrel electromagnetic calorimeter, the energy resolution, σ_E, for beam-momentum electrons from $e^+e^- \to e^+e^-$ events is determined to be approximately $\sigma_E/E \simeq 2.3\%$. For low-energy electrons from the process $e^+e^- \to e^+e^-\gamma$ with momenta between 2 and about 3 GeV, the resolution is given approximately by $\sigma_E/E \simeq 11\%$. Particles penetrating to the electromagnetic calorimeter at $\theta = 90°$ traverse 1.7 radiation lengths of material before reaching it. The effects of this material in front of the calorimeter are included in the energy resolutions quoted. The electromagnetic calorimeter is typically 22 radiation lengths deep, and lead-glass blocks at $\theta = 90°$ subtend 40 by 40 mrad^2.

Outside the electromagnetic calorimeter lies the iron return yoke of the magnet, instrumented

with streamer tubes as a hadron calorimeter. The muon detectors are placed outside the hadron calorimeter. In total, at least seven, and in most regions eight, absorption lengths of material lie between the interaction point and the muon detectors. This material is sufficient that muons produced at the vertex with momenta of less than 2 GeV/c nearly always range out in the absorber, but muons with momenta above 3 GeV/c usually penetrate to the muon detectors. The muon chambers are constructed as two different detector subsystems in the barrel and endcap parts of the detector. They cover 93% of the full solid angle, with gaps for the support structure of the detector, for readout cabling of the inner detector components, and for the beam pipe.

The muon barrel detector covers the polar angle range $|\cos\theta| < 0.7$. It has a cylindrical geometry, composed of 110 planar drift chambers each 1.2 m wide and up to 10.4 m long, positioned at approximately 5 m from the beam axis. The chambers are oriented such that the sense wires lie parallel to the beam axis, so that the drift time provides an r-ϕ coordinate with an accuracy of 1.5 mm. The chambers are arranged with four layers in depth, and are staggered to resolve left-right ambiguities. The z coordinate of hits is measured using charge division between cathode pads as well as the pulse heights at the ends of the sense wires. The overall z resolution obtained is about 2 mm.

The muon endcap detector covers the polar angle range $0.67 < |\cos\theta| < 0.98$. It is composed of two separated planes of limited streamer tube arrays at each end of the detector, approximately 6 m from the interaction point. Each plane contains a set of horizontal and vertical wires each instrumented with horizontal and vertical readout strips with 1 cm pitch. Resolutions of 1–3 mm are obtained on the x and y coordinates of hits using the sharing of charge between strips, and the z coordinate is obtained from the surveyed positions of the chambers.

4 Event Selection and Simulated Data Samples

The data analysed were collected in the 1990 and 1991 data-taking runs of LEP, with centre-of-mass energies ranging between 88.2 GeV and 94.2 GeV. Hadronic Z^0 events were selected using an algorithm described elsewhere [13], additionally requiring that there be at least seven charged tracks in each event. Tracks were counted only if they were reconstructed using at least 20 jet chamber hits, had a measured momentum component in the x-y plane of at least 0.15 GeV/c, a total momentum measured to be less than 65 GeV/c, a distance of closest approach to the beam axis of less than 5 cm, and satisfied other minor quality cuts. The extra track multiplicity requirement is predicted to remove most of the low level of background, particularly Z^0 decays to tau pairs, remaining in the standard hadronic event selection. The hadronic Z^0 event selection efficiency of these requirements is $(98.1\pm0.5)\%$, with a background of less than 0.1%. In addition, the tracking chambers and electromagnetic calorimeters were required to be operating properly when the data were recorded, as were the barrel presampler for the electron analysis, and the muon detectors for the muon analysis. A total of 483 071 and 458 286 hadronic Z^0 decays were selected for the electron and muon analyses respectively.

Three main Monte Carlo samples were used for evaluating acceptances and backgrounds. Events were simulated with the JETSET 7.3 Monte Carlo [14] in conjunction with a computer program that imitated the response of the OPAL detector [15]. Simulated events were processed through the same reconstruction and selection algorithms as data from the detector. The Monte Carlo samples were:

- A sample of 140 000 Z^0 decays to $b\overline{b}$ quarks, used for evaluating the acceptance for muons originating from such events. The fragmentation of the b-flavoured quarks was described by the fragmentation function of Peterson *et al.* [16], with $\epsilon_b = 0.0035$.

- A sample of 56 000 Z^0 decays to $c\overline{c}$ quarks, used for evaluating the background from muons from decays of charm hadrons in the data. The Peterson fragmentation function was used for c-flavoured quarks, with $\epsilon_c = 0.06$.

- A sample of 554 000 hadronic Z^0 decays containing a mixture of all five primary quark flavours. These events were used for evaluating the kinematic acceptance for electrons originating from

$b\overline{b}$ and $c\overline{c}$ decays, for the calculation of the probability of an observed charged track being misidentified as a muon, and to estimate the production rate of prompt leptons produced in events with primary u, d or s quarks. The hadronization properties of all quark flavours were described by the Lund fragmentation function [14]. For b and c quarks a correction was evaluated to account for the different acceptances for the Lund and Peterson fragmentation functions.

The same Monte Carlo samples were also used for determining changes in acceptances for different fragmentation and decay modelling parameters using a reweighting technique. The models and parameter ranges used are discussed in more detail in section 7.

Clusters in the barrel (endcap) electromagnetic calorimeter were associated to a charged track if the track pointed to the cluster centroid within 150 mrad (50 mrad) in θ and 80 mrad (50 mrad) in ϕ. Charged tracks and electromagnetic calorimeter clusters with no associated track were clustered into jets using the JADE algorithm [17] with the E0 recombination scheme [18]. The invariant mass-squared cut-off was set to $x_{\min} = 49\,(\mathrm{GeV}/c^2)^2$. Monte Carlo studies indicated that in order for the jet direction to provide an accurate estimate of the flight direction of the decaying b hadron a cut on $x_{\min}$ was more effective than a cut on the invariant mass-squared scaled by the visible energy (y_{cut}). These studies also led to the specific value of the cut-off taken. The jet axis was found including the momenta of any lepton candidates. The transverse momentum, p_t, of a lepton candidate was determined relative to the axis of the jet containing it.

5 Electron Identification and Backgrounds

Selection Requirements

The electron identification requirements closely followed those used in a previous publication [2]. Charged tracks reconstructed in the central detector were considered as electron candidates in the kinematic and geometrical region defined by

- $p > 2$ GeV/c, $p_t > 0.8$ GeV/c and $|\cos\theta| < 0.7$,

where p is the reconstructed lepton momentum. The requirements on p and p_t were made to enhance the contribution from semileptonic decays of b hadrons. The $\cos\theta$ requirement restricted the angular range for identifying electrons to the uniform barrel region of the detector. Tracks passing these cuts were extrapolated to the lead-glass calorimeter after demanding that at least three hits in the z-chambers were associated to the track to improve the track pointing resolution in θ. This and the remaining electron identification criteria have been motivated in detail elsewhere [2]. The electromagnetic energy included in the cluster associated to the track and contained in the lead-glass blocks with centres lying within a 30 mrad cone around the extrapolated track was found. This energy, E_{cone}, was required to satisfy

- $0.7 < E_{\mathrm{cone}}/p < 1.4$.

A further requirement on the lateral spread of the electromagnetic shower was made:

- $E_{\mathrm{cone}}/(E_{\mathrm{cone}} + \Delta E) > 0.85$ or $\Delta E < 2$ GeV,

where ΔE is the energy contained in all lead-glass blocks adjacent[3] to those defining E_{cone}.

To ensure a reliable measurement of track ionization per unit length, $\mathrm{d}E/\mathrm{d}x$, the track was required to have at least 40 jet chamber charge samples used in the calculation of $\mathrm{d}E/\mathrm{d}x$. It was then demanded that

- $N^{\sigma}_{\mathrm{d}E/\mathrm{d}x} > -2.0$,

[3]The sum $E_{\mathrm{cone}} + \Delta E$ was denoted E_{cone2} in the previous publication [2].

where $N^{\sigma}_{\mathrm{d}E/\mathrm{d}x}$ is a normalized $\mathrm{d}E/\mathrm{d}x$ value defined as

$$N^{\sigma}_{\mathrm{d}E/\mathrm{d}x} = \frac{[\mathrm{d}E/\mathrm{d}x - (\mathrm{d}E/\mathrm{d}x)_0]}{\sigma(\mathrm{d}E/\mathrm{d}x)},$$

$(\mathrm{d}E/\mathrm{d}x)_0$ being the average $\mathrm{d}E/\mathrm{d}x$ for electrons, about 10 keV/cm, and $\sigma(\mathrm{d}E/\mathrm{d}x)$ an estimate of the resolution on $\mathrm{d}E/\mathrm{d}x$ for the candidate track assuming that the track is an electron. Finally, a signal in the presampler with amplitude consistent with an electron was required:

- $N_{\mathrm{pres}} > N_{\mathrm{cut}}$,

where N_{pres} is the presampler amplitude associated to the track (normalized to a value of 2 for beam-energy muons) and N_{cut} is a momentum dependent cut defined as

$$N_{\mathrm{cut}} = 2.5 + p/(2\ \mathrm{GeV}/c) \text{ for } p < 15\ \mathrm{GeV}/c \quad \text{and} \quad N_{\mathrm{cut}} = 10 \text{ for } p > 15\ \mathrm{GeV}/c.$$

After applying all these cuts, the number of identified electrons was $N_{\mathrm{e}}^{\mathrm{tag}} = 6721$.

Background

The electron signal is composed of electrons produced in decays of hadrons containing b and c quarks, and also some from electromagnetic decays of light hadrons. The background consists of hadron tracks misidentified as electrons and electrons produced in photon conversions. The hadronic background was poorly modelled by the detector simulation program, and so it was determined from the data.

The hadronic background was determined from the data in two different ways by fitting the $N^{\sigma}_{\mathrm{d}E/\mathrm{d}x}$ and E_{cone}/p distributions obtained after applying all selection requirements except the $N^{\sigma}_{\mathrm{d}E/\mathrm{d}x}$ and E_{cone}/p cut, respectively. In both cases, the fitting functions were the sum of a background histogram and a Gaussian function approximating the electron signal. The background histogram was obtained directly from the data by making appropriate requirements intended to remove electrons. In the $N^{\sigma}_{\mathrm{d}E/\mathrm{d}x}$ case, the main requirement that biased against electrons was $0.1 < E_{\mathrm{cone}}/p < 0.6$ and in the E_{cone}/p case, $N^{\sigma}_{\mathrm{d}E/\mathrm{d}x} < -3.0$. The parameters of the Gaussian function used to describe the electron $N^{\sigma}_{\mathrm{d}E/\mathrm{d}x}$ distribution were chosen to obtain an optimum description of the data, and no significant momentum dependence of these parameters was detected within present statistics. To obtain the hadronic background only two parameters, the normalization of the background histogram and the normalization of the Gaussian describing the electron signal, were allowed to vary. The number of background events was obtained by counting the number of events in the normalized background histogram inside the region defined by the electron selection cuts. Similar fits were repeated on the E_{cone}/p distributions, but a significant momentum dependence of the mean and width of the Gaussian used to describe the electron E_{cone}/p distribution was included. Both fits, to $N^{\sigma}_{\mathrm{d}E/\mathrm{d}x}$ and E_{cone}/p, yielded compatible background values within errors and the average values were calculated. Examples of the fits are shown in figure 1. The background was calculated in several momentum bins because the hadronic background contamination rises significantly with momentum. The averaged numbers of background tracks, $N_{\mathrm{e}}^{\mathrm{fake}}$, are listed in table 1. The background fractions were calculated separately for 1990 and 1991 data because the addition of the silicon microvertex detector between the two data-taking periods particularly affected the number of photon conversions. The quoted errors include fit normalization errors and errors induced by the uncertainty in the mean and width of the Gaussian distributions. These errors, obtained from independent $N^{\sigma}_{\mathrm{d}E/\mathrm{d}x}$ and E_{cone}/p fits, were determined to be uncorrelated, justifying taking the average of the results of the two fits. The background histogram selection requirements were chosen to reduce any possible correlations, and the data themselves were used to check that any correlation was indeed negligible. In the highest momentum bin, an additional error was added to account for a possible systematic difference between the two fits. Additional systematic errors were studied with different fit ranges and by using slightly different background

p (GeV/c)	1990 Data			1991 Data		
	N_e^{tag}	N_e^{fake}	N_e^{conv}	N_e^{tag}	N_e^{fake}	N_e^{conv}
2–4	388	2.5 $\pm$0.3	65.9$\pm$4.4	1012	3.3 $\pm$0.3	227.1$\pm$11.5
4–6	353	7.3 $\pm$0.6	30.6$\pm$3.1	865	14.6 $\pm$0.9	143.5$\pm$ 8.3
6–10	572	22.9$\pm$1.8	27.1$\pm$4.9	1280	43.3 $\pm$2.5	87.1$\pm$13.7
>10	671	60.7$\pm$5.1	37.7$\pm$7.2	1580	96.7$\pm$9.1	81.2$\pm$14.7
Total	1984	93.4$\pm$5.5	161.3$\pm$15.5	4737	157.9$\pm$9.5	538.9$\pm$40.4

Table 1: Electron signal, hadronic ("fake") background and conversion background as a function of momentum. Both tagged and the estimated number of untagged conversions are included. The errors include only systematic contributions.

selection requirements to determine the uncertainty in the shape of the hadronic background. They were found to be small compared to the other errors and were not included.

Electron candidate tracks originating from photon conversions were identified using an algorithm that searches for pairs of oppositely-charged tracks with a vertex geometry consistent with that expected for a conversion. For each electron candidate, all other tracks in the event with opposite charge were considered as potential partners if they had a specific energy loss $N^{\sigma}_{\mathrm{d}E/\mathrm{d}x} > -2.5$. This $\mathrm{d}E/\mathrm{d}x$ requirement was dropped if the potential partner track had less than 40 available $\mathrm{d}E/\mathrm{d}x$ samples. Projecting both tracks into the x-y plane, the distance of closest approach where the tangents were parallel was found and required to be small. For photon conversions at small radii, where the measurement of θ is more reliable, the difference in θ of the two tracks was required to be small to reduce the combinatorial background. Finally, the pair was tagged as a photon conversion if the distance, r_γ, of the reconstructed conversion to the nominal interaction point satisfied $r_\gamma > 2$ cm, this lower limit being well inside the beam pipe. Distributions of r_γ of tagged photon conversions in the data and in Monte Carlo samples are shown in figure 2, and show good agreement. According to Monte Carlo studies, the efficiency of the photon conversion identification procedure after the previous electron identification requirements is found to be $(84 \pm 4)\%$ for tracks with $p > 2$ GeV/c and $p_t > 0.8$ GeV/c. The efficiency depends only weakly on p, p_t and θ. This efficiency value was used to calculate the number of untagged conversions in the electron sample based on the number of observed photon conversions. Sometimes an electron candidate not originating from a photon conversion is tagged as a conversion due to random pairing of the candidate track with a partner track that fakes the characteristics of a photon conversion. The number of candidate tracks misclassified as conversions was found by taking partner tracks with the same charge as the candidate track, reversing the sign of the curvature of the partner, and then passing the pair through the same tagging algorithm described previously. According to Monte Carlo calculations, this method provides the combinatorial background with 30% accuracy. The combinatorial background obtained in this way is equal to 1.7% of the total number of tagged electrons. Table 1 includes the number of conversion electrons, N_e^{conv}, after removing the combinatorial background and adding the expected number of untagged conversions. The quoted errors include the systematic error in the combinatorial background (30%) and the uncertainty in the efficiency value. The higher conversion rate in 1991 than in 1990 is a consequence of the addition of the silicon microvertex detector and associated material.

Efficiency

The efficiencies of the various electron identification cuts were evaluated using the data, since some of the quantities used in electron identification were poorly simulated by the Monte Carlo. In contrast to the fits for the hadronic background, identified conversions were removed from the electron sample to calculate these efficiencies. Monte Carlo calculations showed that the electron identification

efficiencies differ significantly for each individual source of electrons. The numbers given, determined from the data, are average efficiencies over the various electron sources. Since correlations may exist between the various selection requirements, the efficiency of each was defined as the efficiency of this requirement after all previous cuts have been applied, the order of application being the same as given below. This procedure ensures that the total efficiency is simply the product of all individual efficiencies. The results are listed in table 2, for different momentum intervals. No strong dependence of the efficiencies on p or p_t was observed.

p (GeV/c)	Track quality cuts	$N^{\sigma}_{\mathrm{d}E/\mathrm{d}x}$ cut	E_{cone}/p cut	Lateral spread cut	Pres. cut	Total efficiency
2–4	86.0±2.6	95.7±0.8	89.6±0.6	97.8±0.5	80.8±1.2	58.3±2.1
4–6	85.3±2.3	94.8±0.8	94.6±0.8	92.8±1.0	82.4±1.3	58.5±2.1
6–10	82.6±1.9	94.1±0.8	95.9±1.1	91.2±0.9	82.3±1.1	55.9±1.8
>10	83.0±2.1	94.1±0.8	96.1±1.5	90.6±1.2	76.3±1.4	51.9±2.0

Table 2: Efficiencies, in per cent, of all electron identification requirements as a function of momentum, as evaluated for the 1991 data sample. The errors include both statistical and systematic contributions. Similar efficiencies were obtained for 1990 data.

The efficiency of the additional track quality requirements of z-chamber hit association and number of $\mathrm{d}E/\mathrm{d}x$ hits was determined for tracks passing no other electron identification cut. For this purpose a sample of tracks identified as muons within hadronic events was employed, selected using only the angular deviation between tracks and muon segments described in the next section. Muons are an ideal sample to calculate this efficiency, since the underlying physics processes resulting in muons and electrons are similar once the background has been removed. A correction was applied to account for the background contained in this muon sample. The quoted error includes both the statistical error and the dominant error induced by this background correction.

In the calculation of the efficiency of the $N^{\sigma}_{\mathrm{d}E/\mathrm{d}x}$ requirement, it was found that the $N^{\sigma}_{\mathrm{d}E/\mathrm{d}x}$ distribution depends significantly on the track environment. For this reason, a variable N_{trk} was defined as the average number of additional tracks within the same jet chamber sector as a given track. The average value of N_{trk} is 1.9 for electrons within the kinematic cuts, with a significant momentum dependence. Low momentum pions have a very similar $N^{\sigma}_{\mathrm{d}E/\mathrm{d}x}$ distribution[4] to electrons in the selected kinematic region. At low momenta, a pure pion sample can easily be isolated since the mean $\mathrm{d}E/\mathrm{d}x$ values for different particle species are well separated. The efficiency as a function of N_{trk} was calculated using this sample of pions, and is about 98% for $N_{\mathrm{trk}} < 1$ and decreases below 90% for $N_{\mathrm{trk}} > 4$. The electron efficiencies were obtained by convoluting these efficiency values with the electron N_{trk} distribution. The errors account for uncertainties in the N_{trk} distributions for electrons and also for possible differences between electron and pion $N^{\sigma}_{\mathrm{d}E/\mathrm{d}x}$ distributions.

The efficiency of the E_{cone}/p requirement was measured with electrons with $p < 20$ GeV/c, selected in events with only one good quality track, with $N^{\sigma}_{\mathrm{d}E/\mathrm{d}x} > -1.0$, and no hadronic energy or muon segments associated to the track. This $N^{\sigma}_{\mathrm{d}E/\mathrm{d}x}$ cut was varied between -2.0 and 0.0 and no significant change was observed in the efficiency derived. This event selection, dominated by radiative Bhabha events and two photon processes, provides an almost 100% pure electron sample. To take into account the high multiplicity environment of hadronic events, the extra energy deposited in the calorimeter by surrounding particles was estimated from a distribution of the extra energy surrounding muon candidates in hadronic data events and E_{cone} was corrected appropriately. The correction to the efficiency introduced by this extra energy is smaller than 1%. The effect of incorrect matching of

[4]The quantity $N^{\sigma}_{\mathrm{d}E/\mathrm{d}x}$ was defined for pions by replacing the average electron $\mathrm{d}E/\mathrm{d}x$ value with the expected average $\mathrm{d}E/\mathrm{d}x$ value for pions.

charged tracks to calorimeter energy clusters in hadronic events was also evaluated using Monte Carlo calculations, and found to occur at the level of 2%. The error on this efficiency accounts for the statistical contribution of the single electron sample and the uncertainties from incorrect matching.

To obtain the efficiency of the requirement on the spread of the electromagnetic shower, the hadronic background contained in the electron sample, $N_e^{\rm fake}$, was calculated using a fit, as described earlier, with and without the lateral spread cut, but with all other selection requirements made. The efficiency was defined as:

$$\epsilon(\text{lateral spread}) = \frac{(N_e^{\rm tag} - N_e^{\rm fake})_{\rm lateral\,spread\,cut}}{(N_e^{\rm tag} - N_e^{\rm fake})_{\rm no\,lateral\,spread\,cut}}.$$

Since the presampler requirement was made after the lateral spread requirement, it had to be released for the calculation of this efficiency. This procedure yields satisfactory results at low momenta, but not at high momenta since the background increases considerably after releasing both presampler and lateral spread requirements. For this reason, the presampler cut was applied as well, assuming no correlation between the presampler and lateral spread requirements. It was checked that at low momenta both procedures yielded identical results. At high momenta the check was performed with single electrons as for the $E_{\rm cone}/p$ requirement. The method was applied to both $N^{\sigma}_{{\rm d}E/{\rm d}x}$ and $E_{\rm cone}/p$ distributions and compatible results were found. The total error is the sum of the dominant statistical error, common to both fits, and of the various fit errors, independent for the two methods.

A similar procedure was also used for the determination of the efficiency and error of the presampler requirement.

6 Muon Identification and Backgrounds

Selection Requirements

Charged tracks reconstructed in the central detector were extrapolated through the outer detectors during event reconstruction. Such tracks were considered as possible muon candidates for this analysis only if they satisfied:

- $p > 3$ GeV/c, $p_t > 1.1$ GeV/c and $|\cos\theta| < 0.9$.

The p and p_t requirements enhance the contribution from semileptonic b hadron decays. The numerical values of these cuts differ from those applied to electron candidates because of the different efficiency and background for muon identification. The restriction on polar angle was made to ensure that the tracks were well measured in the central tracking chambers. Tracks were also required to have an impact parameter in the x-y plane, d_0, to the interaction point satisfying $|d_0| < 0.5$ cm. This requirement is expected to have a negligible inefficiency for prompt muons, and rejects some secondary muons from decays of pions and kaons.

The points of closest approach of each extrapolated track to track segments reconstructed independently in the muon detectors were examined. The angular separation of these points and the muon segments was calculated in azimuthal and polar angle. The sum in quadrature of these deviations, normalized by their errors, was calculated, and is denoted $\chi_{\rm pos}$. In case of ambiguous multiple matches between extrapolated tracks and muon segments, the muon segment with the lowest $\chi_{\rm pos}$ for a given track was associated to that track. In the case where this still left several tracks matched to a single muon segment, only the track extrapolating closest in angle to the segment was considered. The distribution of the $\chi_{\rm pos}$ measure is shown in figure 3 for low-multiplicity muon pair events, and for hadronic Z^0 decays. Muon candidates were required to satisfy:

- $\chi_{\rm pos} < 3$.

- No more than twenty muon segments should be found in an azimuthal slice of 300 mrad around the track. This requirement rejected preferentially detector noise and hadronic showers penetrating to the muon chambers.
- $\mathrm{d}E/\mathrm{d}x$, measured in the jet chamber, must be consistent with that of a muon. Candidates were rejected only if they had at least 20 jet chamber charge samples used in the calculation of $\mathrm{d}E/\mathrm{d}x$, and the $\mathrm{d}E/\mathrm{d}x$ measured was lower than a value corresponding to two standard deviations below that expected for a muon. This energy loss requirement removes mostly $\mathrm{K}^{\pm}$ tracks matched to muon segments—the ionization losses of muon and charged pion tracks are not sufficiently separated in the momentum range of interest.

A total of 7249 muon candidates passed all these requirements.

Background

Hadronic background to the prompt muon signal originates predominantly, in this analysis, from the decays in flight of light hadrons, particularly $\pi^{\pm}$ and $\mathrm{K}^{\pm}$. Additional contributions arise from leakage of hadronic showers through to the muon detectors ("punchthrough"), hadrons which pass through the detector material without interacting strongly ("sailthrough"), and from random incorrect association of a charged track with a reconstructed muon segment caused by some other particle. All these processes together are referred to as the hadronic background to the prompt muon signal.

The amount of hadronic background in the muon sample was evaluated in a two-step process. Monte Carlo simulated events were used to measure the probability that a track reconstructed in the central tracking chambers was incorrectly identified as a prompt muon. This fake probability per track was then multiplied by the number of charged tracks seen in the data to obtain the total hadronic background in the sample. This procedure largely removes sensitivity to the Monte Carlo simulation of the p and p_t distributions of all tracks. The Monte Carlo modelling of the fake probabilities was tested using various samples of tracks with low prompt muon content, described below. Small corrections to the fake probabilities were derived from these studies, as was the uncertainty on the amount of background.

In the sample of muons selected by the cuts listed above, the level of hadronic background was estimated to be approximately 11%. Of this, roughly two-thirds is expected to come from decays in flight, 15% from punchthrough, and the remainder from sailthrough and incorrect associations. Approximately 75% of the background tracks are predicted to be charged pions, and 20% to be charged kaons.

The accuracy of the Monte Carlo modelling of the fake probability per track was studied by comparing Monte Carlo predictions with data in various control samples. The same selections were applied to data and simulated events for each of the samples, and the accuracy of modelling of track yields and matching distributions was tested. The background from charged pions was tested with identified $\mathrm{K}^0 \to \pi^+\pi^-$ decays, complemented by $\tau \to 3\pi$ decays in $\mathrm{Z}^0 \to \tau^+\tau^-$ events. The χ_{pos} distribution of a track sample enhanced in kaons and protons was studied with a sample of tracks passing all the muon identification requirements, except failing the $\mathrm{d}E/\mathrm{d}x$ cut. The modelling of tracks matched incorrectly between central tracking chambers and muon detectors was studied with samples passing the muon identification cuts except failing the $\chi_{\mathrm{pos}} < 3$ requirement, or failing the criteria used to resolve matching ambiguities. The corrections derived from these studies were typically less than 10%. While a wide range of control samples was available, not all components of the hadronic background could be tested individually, so the quoted uncertainty contains an estimate of the remaining ambiguity, as well as contributions from the statistical precision of the test samples. The most important background components for this analysis, namely pion and kaon decays in flight, were assigned relative errors of about $\pm 10\%$. Punchthrough background, which predominates only at very high momentum, was attributed a $\pm 50\%$ error. This is the most difficult background to simulate, because it depends on details of hadronic shower development through the detector material.

The modelling of the relative yields of $\pi^{\pm}$ and $K^{\pm}$ by the Monte Carlo is a possible additional source of uncertainty. However, with the muon identification criteria listed above, this is not expected to be a significant source of error, because after the dE/dx requirement the fake probabilities per track for the two particle types are the same to within 30%. The background prediction is more sensitive to the modelling of the relative yield of proton tracks, but the relatively small number of protons means that this too is assessed not to be an important source of error.

For the sample used in this analysis, the overall fake probability predicted by the Monte Carlo was corrected by multiplying by 0.98, and was assigned a relative error of $\pm$14%. The average fake probability per charged track was found to be (0.45 ± 0.06)%, varying rather slowly with p and p_t. This gave a total hadronic background in the muon sample of 769 ± 104 tracks, where the error includes systematic uncertainties.

Efficiency

The modelling of muons in the OPAL detector was studied using muon-pair events, and was found to be well reproduced by the detector simulation. This allowed the muon identification efficiency in hadronic events to be determined from Monte Carlo events processed through the detector simulation program. Indeed the overall value of the muon identification efficiency did not need to be calculated for this analysis, rather muon candidates in simulated events were counted in the same way as data, to derive overall acceptances with the muon identification efficiencies folded in. Nevertheless, studies of the reproducibility of the data by the Monte Carlo simulation were made in order to assess the systematic uncertainty on the identification efficiency.

The matching requirement, $\chi_{\rm pos}< 3$, removes roughly 20% of prompt muons passing the p, p_t and $|\cos\theta|$ cuts. The inefficiency arises largely from the geometrical acceptance of the muon chambers, and also includes multiple scattering and calibration effects. The simulation of the effect of the $\chi_{\rm pos}$ cut was checked using muon pairs from two-photon scattering processes, and $Z^0 \to \mu^+\mu^-$ decays. These tests provide good control of the combined effects of modelling of multiple scattering, of gaps in the muon chamber acceptance and of chamber calibration. Events from two-photon scattering processes with $\mu^+\mu^-$ final states were selected by requiring exactly two charged tracks with two-particle invariant mass above 2 GeV/c^2, and that one track be identified as a muon. The same criteria were applied to data and simulated two-photon events, and the modelling of the efficiency of identifying the other track as a muon was evaluated. Decays of the type $Z^0 \to \mu^+\mu^-$ were identified using a standard selection procedure described elsewhere [13]. This algorithm has an efficiency very close to 100% with very low backgrounds, resulting in negligible selection biases, so that both muons could be used to test the accuracy of the muon identification modelling. For these well-isolated muon candidates, the detector simulation was found to model the efficiency of the $\chi_{\rm pos}$ cut well, with a relative error of 2.5%. In hadronic Z^0 decays there are additional small inefficiencies expected from possible incorrect association of tracks to muon segments, and from failure to reconstruct muons as charged tracks. The sizes of these effects were estimated using Monte Carlo simulation to be an additional 2% and less than 1% efficiency loss respectively. A 2.5% additional uncertainty was ascribed due to these effects.

With perfect calibration, the dE/dx requirement would remove 2.5% of the remaining prompt muons. Modelling of dE/dx, and thus the actual effect of the cut, was studied using identified charged pion samples. Corrections for the effects of nearby tracks on the measured dE/dx were obtained from a data sample of low momentum pions. They were applied to the data as a function of $N_{\rm trk}$. In addition, it was found that a degradation of the resolution was needed for a small fraction of tracks in simulated events in order to reproduce the dE/dx distributions as a function of $N_{\rm trk}$ seen in the data. After applying these corrections, the systematic uncertainty remaining on the effect of the dE/dx cut was estimated with identified $K^0 \to \pi^+\pi^-$ decays. A residual systematic uncertainty of 1% was found, compared to the 2.5% of muons rejected by the dE/dx cut.

The muon segment multiplicity and d_0 cuts are estimated to be more than 99% efficient for prompt muons, with uncertainties negligible compared to those of the $\chi_{\rm pos}$ and dE/dx cuts. Overall, the muon

identification efficiency was found to be approximately 76%, although as discussed above, the precise value of this number is not used in this analysis. Overall, the muon identification efficiency was assessed to have a relative systematic uncertainty of $\pm 3.7\%$.

7 Modelling and Branching Ratio Studies

This measurement of $\Gamma_{b\bar{b}}/\Gamma_{had}$ requires a good understanding of heavy quark fragmentation, the momentum spectra of leptons from the semileptonic decay of b and c hadrons, and the corresponding semileptonic branching ratios. These are discussed in turn, the latter two in some detail because they potentially give rise to the largest systematic uncertainties on the final result.

In addition, a value of $\Gamma_{c\bar{c}}/\Gamma_{had}$ is needed to extract $\Gamma_{b\bar{b}}/\Gamma_{had}$. Measurements available [3,4,8,19–21] are consistent with Standard Model predictions, namely 0.171 as obtained from the ZFITTER program [22] (with top quark and Higgs boson masses of 150 and 300 GeV/c^2 respectively, and $\alpha_s = 0.12$). The most precise published measurement [19] comes from the yield of high momentum D^* mesons, and has a fractional error of $\pm 22\%$. Since D^* mesons are also produced in b hadron decays, this measurement also depends on $\Gamma_{b\bar{b}}/\Gamma_{had}$. To remove the consequent circularity, for this measurement of $\Gamma_{b\bar{b}}/\Gamma_{had}$ the Standard Model value of $\Gamma_{c\bar{c}}/\Gamma_{had} = 0.171$ was used. A fractional error of 22% was taken on this number, to represent the accuracy of current measurements of $\Gamma_{c\bar{c}}/\Gamma_{had}$.

Heavy Quark Fragmentation

The fragmentation of the heavy quark (b or c) affects mostly the acceptance of the lepton momentum cut. The acceptance of this cut is large for both the electron and muon channels when the p_t requirements have been made. The fragmentation functions for both b and c quarks have been measured at LEP, using charged leptons [3–5,7,23] and reconstructed D^* mesons [19,20]. These results are usually expressed in terms of the mean fraction of the beam energy carried by the heavy hadron produced in the fragmentation process, $\langle x_E \rangle$. The measurements listed above are averaged to obtain $\langle x_E \rangle = 0.51 \pm 0.02$ for c quarks, and $\langle x_E \rangle = 0.70 \pm 0.02$ for b quarks. The ranges correspond to $\epsilon_c = 0.05 \pm 0.02$ and $\epsilon_b = 0.0055^{+0.0040}_{-0.0030}$ when interpreting the measurements in terms of the Peterson fragmentation function inside the JETSET 7.3 framework. Other forms of fragmentation function were not considered explicitly because the uncertainty on $\Gamma_{b\bar{b}}/\Gamma_{had}$ resulting from heavy quark fragmentation is small (see below).

Models of Semileptonic Heavy Hadron Decays

The kinematic acceptances of the p and p_t cuts for prompt leptons produced by different heavy hadron decays depend, for each channel, on the lepton momentum spectrum in the rest frame of the decaying heavy hadron. Several models predict these spectra, and were used to estimate the size of the resulting systematic uncertainties. The effects of different lepton spectra are important not only at LEP, but also in experiments at lower energies which make measurements of the semileptonic branching ratios. For this analysis the $b \to \ell$ and $b \to c \to \ell$ branching ratios measured by the CLEO Collaboration [10] were taken because they repeated their analysis with different decay spectra and quote the separate results explicitly. The measurements were made using decays of the $\Upsilon(4S)$, which produce only B^0 and B^+ mesons. Employment of these results therefore needs special consideration of the extra particles B_s and Λ_b produced at LEP. The $\Upsilon(4S)$ decays to B mesons which are practically at rest in the CLEO detector. Experimental difficulties identifying low momentum electrons and muons mean that the CLEO analysis is most sensitive to leptons with rest-frame momenta in the upper half of the decay momentum spectrum. This introduces a strong correlation between measured branching ratios and decay model. In the analysis described here the requirement of high transverse momentum introduces an acceptance similarly biased towards high lepton momenta in the decaying b hadron rest frame. Inclusion of the CLEO branching ratio measurements appropriate to each decay

model therefore results in a reduced overall uncertainty on the acceptance for b decays, because of this sensitivity of the CLEO and OPAL analyses to the same region of the lepton rest-frame momentum spectrum.

Following CLEO, two models of heavy flavour decays were considered, referred to as ACCMM and ISGW. The ACCMM model [24] is a free-quark model refined by inclusion of QCD corrections. It has two input parameters, a Fermi momentum parameter, p_F, and the mass, m, of the quark produced in the heavy quark decay. For semileptonic decays of b hadrons, the same values of these parameters were adopted as in the CLEO analysis ($p_F = 298$ MeV/c, $m_c = 1673$ MeV/c^2). The ISGW model [25] is based on a form-factor calculation of an explicit sum of spectra calculated for individual three-body final states. There are no free parameters in the model. In addition to these two models, CLEO also measured $B(b \to \ell)$ with a modified version of the ISGW model, referred to as ISGW**. In fitting this modified model to the CLEO data, the fraction of semileptonic $b \to \ell$ decays via the reaction $\overline{B} \to D^{**}\ell\nu$ was allowed to float freely, where D^{**} represents a sum over the four excited D states with one unit of orbital angular momentum. In the unmodified ISGW model the fraction of these D^{**} decays is 11%. The ISGW** model contains a 32% D^{**} fraction from the result of this fit.

The effect of uncertainties in the momentum spectrum of leptons from semileptonic c decays was also included. The spectra predicted by the ACCMM (with $p_F = 282$ MeV/c, $m_s = 50$ MeV/c^2, from a fit [10] to DELCO data [26]) and ISGW models were considered. Compared to the DELCO data, the rest-frame momentum spectrum for $c \to \ell$ decays predicted by JETSET was found to be too soft, largely due to an excessive fraction of 4- and 5-body semileptonic D decays in the JETSET decay tables.

Cascade decays $b \to c \to \ell$ require a more involved treatment, because reliable models do not exist for the inclusive $b \to c$ decay. The $b \to c \to \ell$ spectra were derived [10] using a CLEO measurement of the momentum spectrum of D mesons reconstructed in B decays [27], folded with the ACCMM or ISGW predictions for the momentum spectrum of the lepton in the decaying c hadron rest frame. When fitting the predicted lepton spectra to their data, CLEO consistently took either both ACCMM $b \to \ell$ and $b \to c \to \ell$ predictions, or both ISGW spectra. The same pairing of $b \to \ell$ and $b \to c \to \ell$ spectra was taken for this analysis. When considering the ISGW** model for $b \to \ell$ decays, the $b \to c \to \ell$ decay spectrum was taken to be that predicted by the ISGW model for the $c \to \ell$ decays.

In practice, different decay models were simulated by reweighting from the rest-frame momentum spectrum obtained from the JETSET Monte Carlo to the desired spectrum. A reweighting technique was necessary because full detector simulation of sufficient events according to the different models would have required more computer resources than were available. For $b \to \ell$ and $b \to c \to \ell$ decays, leptons were reweighted according to their momentum in the decaying b hadron rest frame. The rest-frame momentum spectra of both semileptonic and cascade b decays were simultaneously reweighted to each model. B_s and Λ_b hadron decays were reweighted by the same momentum-dependent factors as B^+ and B^0 decays. The masses of B_s and Λ_b particles were taken to be 5.48 and 5.62 GeV/c^2, respectively. The variation of the c semileptonic decay model was considered independently from the $b \to \ell$ decay model and the $c \to \ell$ branching ratio, since correlated measurements have not been made of any of the different quantities. The effects on the momentum spectra of radiative corrections in the heavy hadron decay [28], different for electrons and muons, are included in the reweighting procedure. Also included in the $b \to \ell$ decay spectrum are the contributions of $b \to u\ell\nu$ decays, normalized by branching ratios measured by CLEO in the fits described above. The momentum spectra of muons in the decaying b or c hadron rest frame are shown in figure 4 for the $b \to \ell$, $b \to c \to \ell$ and $c \to \ell$ decay chains, for different models.

The $b \to \ell$ and $b \to c \to \ell$ Branching Ratios

The CLEO measurements of $B(b \to e)$ and $B(b \to c \to e)$ were adopted, assuming that the branching ratios for $b \to e$ and $b \to \mu$, and for $b \to c \to e$ and $b \to c \to \mu$, are equal. CLEO also measured $B(b \to \mu)$ from their muon momentum spectrum, but experimental difficulties in identifying

low momentum muons did not allow a measurement of $B(\mathrm{b} \to \mathrm{c} \to \mu)$. Additionally a measurement of $B(\mathrm{b} \to \ell)$ and $B(\mathrm{b} \to \mathrm{c} \to \ell)$ was made from the combined electron and muon data, but the large experimental systematics on the CLEO muon data resulted in greater overall systematic uncertainties compared to the measurements using electrons alone. This procedure differs from that adopted in the previous publication [2] where the CLEO measurements of the $\mathrm{b} \to \ell$ and $\mathrm{b} \to \mathrm{c} \to \ell$ branching ratios were used.

Use of branching ratio measurements made in $\Upsilon(4S)$ decays in this analysis leads to additional uncertainties due to the admixture of $\mathrm{B_s}$ and Λ_b particles at LEP. For $B(\mathrm{B^0},\mathrm{B^+} \to \ell)$ measured with electrons, the CLEO central result with the ACCMM model is $(10.5 \pm 0.2 \pm 0.3)\%$ [10], an overall 3.4% relative error. While first measurements of the yields of semileptonically decaying $\mathrm{B_s}$ and Λ_b hadrons have been made recently [29], their precision is not sufficient to be useful for this analysis without further constraints. Some theoretical arguments suggest that the semileptonic branching ratios of the different weakly decaying b hadrons should vary by about 10% [30]. With such a variation, either broad assumptions about the relative abundances of b hadrons can be made, or the measured product branching fractions [29] can be included to constrain the possible effect on the average $B(\mathrm{b} \to \ell)$ in $\mathrm{Z^0}$ decays.

Naïvely it is expected that the fraction of $\mathrm{B_s}$ mesons will be less than that of $\mathrm{B^0}$ and $\mathrm{B^+}$ (which are assumed to have equal abundances), and hence to be bounded by 33%. The fraction of Λ_b might be expected to be less than 20%. Such limits, together with up to 10% different branching fractions, lead to uncertainties of around 4% on the branching ratio $B(\mathrm{b} \to \ell)$.

The measured product branching fractions for $\mathrm{B_s}$ and Λ_b production and decay already made at LEP [29] can reduce this uncertainty slightly. Combining the measured numbers from OPAL and ALEPH, using $B(\Lambda_\mathrm{c} \to \mathrm{pK^-}\pi^+) = (3.2 \pm 0.7)\%$ and $B(\mathrm{D_s} \to \phi\pi) = (2.8 \pm 0.5)\%$ [31], the branching ratio products

$$\begin{aligned} f(\mathrm{b} \to \mathrm{B_s}) B(\mathrm{B_s} \to \mathrm{D_s} \ell \nu X) &= (1.6 \pm 0.5)\% \\ f(\mathrm{b} \to \Lambda_\mathrm{b}) B(\Lambda_\mathrm{b} \to \Lambda_\mathrm{c} \ell \nu X) &= (2.0 \pm 0.7)\% \end{aligned}$$

are obtained, where $f(\mathrm{b} \to \mathrm{B_s}, \Lambda_\mathrm{b})$ represents the probability that a b quark hadronizes into a hadron $\mathrm{B_s}$ or Λ_b. From these measurements, 90% confidence level limits on these branching ratio products of 2.2% and 2.8%, respectively, are obtained. The effect of 10% shifts of the $B(\mathrm{b} \to \ell)$ for $\mathrm{B_s}$ or Λ_b, requiring that the total fractions of $\mathrm{B^+}$, $\mathrm{B^0}$, $\mathrm{B_s}$ and Λ_b total one, and that the fractions of $\mathrm{B^+}$ and $\mathrm{B^0}$ are the same, give fractional shifts of $\pm 2.1\%$ and $\pm 2.7\%$ respectively in the overall value of $B(\mathrm{b} \to \ell)$. Adding these shifts in quadrature gives a 3.4% relative error on $B(\mathrm{b} \to \ell)$ from the uncertain mixture of b hadrons. Any uncertainty in these numbers due to the uncertainty in $\Gamma_{\mathrm{b\bar{b}}}/\Gamma_{\mathrm{had}}$ is negligible compared to the experimental errors on the yields of semileptonically decaying $\mathrm{B_s}$ and Λ_b hadrons.

The CLEO measurement of the branching ratio product for $B(\mathrm{b} \to \mathrm{c} \to \mathrm{e})$ with the ACCMM decay model is $(9.7 \pm 0.8 \pm 0.6)\%$ [10], namely a 10.3% fractional error. Production of Λ_b and $\mathrm{B_s}$ states at LEP has the effect of altering this branching ratio, since the Λ_c and $\mathrm{D_s}$ states expected to be produced dominantly from Λ_b and $\mathrm{B_s}$ decays, respectively, have smaller semileptonic branching fractions than the mixture of c hadrons produced from $\mathrm{B^0}$ and $\mathrm{B^+}$ decays. Using abundances measured by CLEO [27] of c hadrons from $\mathrm{B^0}$ and $\mathrm{B^+}$ decays, and assuming that $\mathrm{B_s}$ and Λ_b hadrons decay to $\mathrm{D_s}$ and Λ_c hadrons respectively, leads to shifts of typically 7% from the $B(\mathrm{b} \to \mathrm{c} \to \mathrm{e})$ value measured at CLEO to that expected at LEP. Since the analysis is not very sensitive to this number, a correction of 0.93 ± 0.07 is applied to the CLEO $B(\mathrm{b} \to \mathrm{c} \to \mathrm{e})$ measurement, where the uncertainty is conservatively taken to be the full size of the effect. Allowing widely different fractions of $\mathrm{B_s}$ and Λ_b to be produced relative to $\mathrm{B^0}$ and $\mathrm{B^+}$ leads to correction factors which are covered by the 0.07 error quoted. For the ACCMM model, this results in a $\mathrm{b} \to \mathrm{c} \to \ell$ branching ratio of $(9.0 \pm 1.2)\%$. The branching ratio values used for the different models are summarized in table 3.

Decay mode	ACCMM	ISGW	ISGW**
$b \to \ell$	10.50 ± 0.50	10.1	11.1
$b \to c \to \ell$	9.0 ± 1.2	10.3	8.6
$b \to J/\psi \to \ell$	0.14 ± 0.04		
$b \to \tau \to \ell$	0.5 ± 0.2		
$c \to \ell$	9.6 ± 1.1		

Table 3: Branching ratios, in per cent, derived for the different b and c hadron decays in Z^0 decays, for different semileptonic decay models. The ACCMM model is used to obtain the central result.

The $b \to J/\psi \to \ell$ Branching Ratio

Combining the measured branching ratios for $B^0, B^+ \to J/\psi$ and $J/\psi \to \ell^+\ell^-$ decays [31] gives for $\ell^+\ell^-$ and inclusively for leptons ℓ:

$$\begin{aligned} B(B^0, B^+ \to J/\psi \to \ell^+\ell^-) &= (0.07 \pm 0.01)\% \\ B(B^0, B^+ \to J/\psi \to \ell) &= (0.14 \pm 0.02)\%. \end{aligned}$$

The unknown effect of B_s and Λ_b decays is included by adding an additional 25% uncertainty to this branching ratio. The overall branching ratio, $B(b \to J/\psi \to \ell) = (0.14 \pm 0.04)\%$, gives only a small uncertainty on $\Gamma_{b\bar{b}}/\Gamma_{had}$.

The $b \to \tau \to \ell$ Branching Ratio

The branching ratio of b to τ relative to b to e is predicted by the quark model [32] from phase space arguments. Allowing b and c quark masses to vary in the ranges 4.8–5.2 GeV/c^2 and 1.3–1.7 GeV/c^2, respectively, gives a prediction for the relative τ and e branching ratios of (25$\pm$10)%. More sophisticated form-factor calculations [33] do not change this conclusion. Using the well-measured $B(\tau \to e) = (17.9 \pm 0.3)\%$ [31] gives $B(b \to \tau \to \ell) = (0.5 \pm 0.2)\%$, where differences between measurements of $B(b \to \ell)$ for different decay models have been neglected. These numbers are consistent with a recent measurement of the branching ratio for $b \to \tau\overline{\nu}_\tau X$ by the ALEPH collaboration [34]. The uncertainty on $\Gamma_{b\bar{b}}/\Gamma_{had}$ resulting from the uncertainty on $B(b \to \tau \to \ell)$ is small.

The $c \to \ell$ Branching Ratio

For semileptonic decays of c hadrons, the overall branching ratio is calculated considering the measured branching ratios and lifetimes of the separate hadron types. The semileptonic branching ratios and lifetimes of D^0 and D^+ mesons are well measured [31], and the lifetimes of D_s and Λ_c states are also known with better than 10% precision. If the semileptonic partial widths of all these c hadrons are assumed to be the same, the semileptonic branching ratios are just proportional to the particle lifetimes. Combining the different measurements with the JETSET prediction for the relative abundances D^+:D^0:D_s:Λ_c of 25:54:12:8 gives a predicted average semileptonic branching ratio for a c hadron from Z^0 decay to be (9.6$\pm$0.9)%, including the errors on the measured branching fractions and lifetimes. Varying the vector to scalar meson production ratio in the range 2.5:1 to 4:1, and the fractions of produced D_s and Λ_c hadrons between 10–20% and 5–15% respectively, leads to an additional error of $\pm$0.6% on the average $B(c \to \ell)$. Overall, this gives $B(c \to \ell)$=(9.6$\pm$1.1)%. The variation of the $c \to \ell$ branching ratio is considered independently of the $b \to c \to \ell$ branching ratio, because different mixtures of c hadrons are involved.

8 Results

Electrons

As discussed above, the electron identification efficiency was determined from the data themselves, as an average over all prompt electron sources. The background-subtracted number of identified electrons in the data was therefore corrected for the identification efficiency before subdivision into the contributions from the different prompt electron sources. The number of electrons inside the kinematic and geometrical cuts defined above was calculated in the four momentum bins introduced in section 5 by subtracting the hadronic and conversion background ($N_e^{\rm fake}$ and $N_e^{\rm conv}$), and correcting for the electron identification efficiency ($\epsilon_{\rm elec}$):

$$N_e^{\rm corr} = (N_e^{\rm tag} - N_e^{\rm fake} - N_e^{\rm conv})/\epsilon_{\rm elec}.$$

Using the values listed in tables 1 and 2 and adding all momentum bins, a rate of prompt electrons passing the p, p_t and $\cos\theta$ cuts of

$$N_e^{\rm corr}/N_{\rm had} = (2.070 \pm 0.028 \pm 0.063)\%$$

was derived, where the first error is statistical and the second systematic, and where $N_{\rm had}$ is the number of Z^0 decays selected by the hadronic event selection, 483071, divided by the efficiency of that selection, namely (98.1±0.5)%. Some systematic errors are correlated from momentum bin to momentum bin. This correlation was taken into account to obtain the total systematic error. The approximate expected breakdown of the various prompt electron sources is given in table 4. The distributions of p and p_t for prompt electrons, after correction for backgrounds and efficiency, are shown in figure 5.

$b \to e$	74 %
$b \to c \to e$	13 %
$b \to J/\psi \to e$	1 %
$b \to \tau \to e$	1 %
$c \to e$	9 %
others	2 %

Table 4: Expected fractions of different sources of prompt electrons passing the momentum and transverse momentum cuts.

The rate of electrons from $c \to \ell$ decays was estimated to be

$$N_e^{\rm c}/N_{\rm had} = (0.183 \pm 0.051)\%.$$

For the value of $N_e^{\rm other}/N_{\rm had}$ the following value, obtained from JETSET 7.3 simulated events, was taken:

$$N_e^{\rm other}/N_{\rm had} = (0.043 \pm 0.010)\%,$$

where the error includes effects such as the uncertainties in the π^0 and η yields [35], and a ±100% uncertainty on the small number of leptons originating from b and c quarks produced in fragmentation processes. The Dalitz decays contributing to $N_e^{\rm other}/N_{\rm had}$ are more likely to be flagged as photon conversions than prompt electrons from other sources, and have been scaled down by 20% to account for this effect, according to Monte Carlo predictions.

One source of experimental systematic uncertainty specific to the electron channel concerned the effect of radiation losses of electrons inside the tracking chamber volumes. Such losses reduce the

electron momentum, and thus lead to a reduced kinematic efficiency for electrons to pass the p and p_t cuts. This effect amounts to an 8% correction for electrons, evaluated using the detailed simulation of the detector performed for Monte Carlo events. The effects of the material within the tracking chambers were simulated with an accuracy of about 10%, leading to an error of 0.8% on $\Gamma_{b\bar{b}}/\Gamma_{had}$ from this source.

The value of $\Gamma_{b\bar{b}}/\Gamma_{had}$ was calculated from

$$\left.\frac{\Gamma_{b\bar{b}}}{\Gamma_{had}}\right|_e = \frac{N_e^{corr} - N_e^c - N_e^{other}}{2N_{had}\sum(B\cdot\epsilon)_b}.$$

The sum $\sum(B\cdot\epsilon)_b$ was calculated from Monte Carlo to be (4.25±0.24)%. The central value was obtained with the ACCMM model for semileptonic decays, and using the central values of fragmentation parameters and branching ratios listed in section 7. The error includes branching ratio, fragmentation, and decay model uncertainties. The result obtained was:

$$\left.\frac{\Gamma_{b\bar{b}}}{\Gamma_{had}}\right|_e = 0.216 \pm 0.003 \pm 0.007 \pm 0.012,$$

where the first error is statistical, the second arises from detector performance uncertainties, and the third from uncertainties from fragmentation, branching ratios and decay models. The detector performance systematic error includes electron identification and background uncertainties, that from electron radiation losses, and those from the hadronic Z^0 event selection and Monte Carlo statistics. The error sources are summarized in table 5, where they are explicitly divided into those uncorrelated or correlated between the electron and muon analyses.

Muons

Unlike for the electron channel, the muon identification efficiencies are calculated folded in with the kinematic and geometrical acceptances, using simulated events. The number of tracks passing all cuts, N_μ^b, expected from prompt muons in $Z^0 \to b\overline{b}$ decay events is calculated from the number of observed muon candidates in the data, N_μ^{tag}:

$$N_\mu^b = N_\mu^{tag} - N_\mu^{fake} - N_\mu^c - N_\mu^{other}.$$

A total of $N_\mu^{tag} = 7249$ identified muon candidates passed all cuts. The predicted contribution from hadronic background to the prompt muon signal was $N_\mu^{fake} = 769\pm104$ tracks. Decays of the type $c \to \ell$ were predicted to contribute $N_\mu^c = 332\pm82$ tracks, where the error is the full systematic uncertainty. An estimate of $N_\mu^{other} = 25\pm25$ muons was obtained from the simulated JETSET 7.3 events for the contribution from b and c quarks produced in fragmentation processes. Subtraction of these contributions left an estimated

$$N_\mu^b = 6123 \pm 85 \pm 135$$

prompt muons in the data coming from $Z^0 \to b\overline{b}$ decay events, where the first error is statistical and the second systematic. The estimated fractions of muon candidates in the sample from the different sources are given in table 6. The p and p_t distributions of the muon candidates are shown in figure 6.

The accuracy of detector modelling by the simulation program is reflected in the muon identification efficiency and background uncertainties, as well as in the error on the hadronic Z^0 event selection efficiency. An additional source of systematic uncertainty on the kinematic acceptance arose due to the description of the polar angle resolution of tracks, and was estimated to lead to a small additional uncertainty of ±0.4%. This error does not apply to the electron analysis because z-chamber hits are required as part of the electron identification requirements.

The fraction of hadronic Z^0 decays to $b\overline{b}$ pairs was calculated from

$$\left.\frac{\Gamma_{b\bar{b}}}{\Gamma_{had}}\right|_\mu = \frac{N_\mu^b}{2N_{had}\sum(B\cdot\epsilon)_b},$$

Error source	Electrons	Muons	Combined
Lepton ID efficiency	2.9	3.7	2.3
Hadronic backgrounds	0.2	1.7	0.8
Conversion background	0.9	-	0.5
Monte Carlo statistics	1.1	1.2	0.8
Electron radiation losses	0.8	-	0.4
Polar angle determination	-	0.4	0.2
Total uncorrelated	3.3	4.3	2.7
Hadronic Z^0 selection	0.5	0.5	0.5
$\Gamma_{c\bar{c}}/\Gamma_{had}$	1.9	1.2	1.6
$c \to \ell$ branching ratio	1.0	0.6	0.8
c quark decay model	0.9	0.5	0.7
c quark fragmentation	0.8	0.3	0.6
CLEO $b \to \ell$ branching ratio	2.8	3.0	2.9
$B(b \to \ell)$ from Λ_b and B_s	2.8	3.0	2.9
$b \to c \to \ell$ branching ratio	1.9	1.0	1.5
$b \to J/\psi \to \ell$	0.5	0.4	0.5
$b \to \tau \to \ell$	0.6	0.4	0.5
b quark decay model	0.5	0.3	0.4
b quark fragmentation	1.4	1.2	1.3
Other lepton sources	0.5	0.4	0.5
Total correlated	5.4	4.9	5.1
Total systematic	6.3	6.5	5.7
Statistical	1.4	1.4	1.0

Table 5: Summary of effects, in per cent, of the different error sources on the electron, muon and combined $\Gamma_{b\bar{b}}/\Gamma_{had}$ results.

$b \to \mu$	76 %
$b \to c \to \mu$	7 %
$b \to J/\psi \to \mu$	1 %
$b \to \tau \to \mu$	1 %
$c \to \mu$	5 %
hadronic background	11 %

Table 6: Expected fractions of muon candidates from different sources in the final sample.

where, unlike in the electron case, the acceptances ϵ include the muon identification efficiency as well as the kinematic and geometrical effects. The number of hadronic Z^0 decays, N_{had}, was calculated from the number selected in the data, 458 286, divided by the selection efficiency, (98.1±0.5)%. The sum $\sum(B \cdot \epsilon)_b$ was calculated to be (2.92±0.17)% from Monte Carlo studies, taking the same central

assumptions and errors as for the electron channel. The final result obtained using muons was:

$$\left.\frac{\Gamma_{b\bar{b}}}{\Gamma_{had}}\right|_{\mu} = 0.224 \pm 0.003 \pm 0.010 \pm 0.011,$$

where the first error reflects the statistics of the data, the second the systematic errors arising directly from OPAL detector-related uncertainties, and the third includes all systematic effects due to b and c quark and hadron modelling. The individual systematic uncertainties are listed in table 5. The detector-related uncertainty quoted includes the errors due to muon background and identification, hadronic Z^0 decay acceptance, detector simulation uncertainties, and Monte Carlo statistics.

Further Checks of Results

The selection cuts on the p and p_t of lepton candidates were chosen to give a small total fractional error on $\Gamma_{b\bar{b}}/\Gamma_{had}$. Lowering the momentum cut results in an increase in the background fraction, and increasing the momentum cut results in an increase of the fragmentation errors. A lower p_t cut has the effect of increasing the cascade and fragmentation errors as well as those from charm, and a higher cut rapidly results in loss of statistics. For both channels it was checked that changes in the cuts over wide ranges did not lead to significant changes in the result.

Consistent results were obtained when the sample was divided into the two data-taking years, 1990 and 1991. The effect of including the data taken with collision energies not at the Z^0 mass, but up to 3 GeV away, was assessed to be less than 0.4%, and was neglected.

Combination of Results

The central values from the electron and muon analyses, 0.216 and 0.224 respectively, differ by less than one standard deviation of the uncorrelated errors, and so are compatible. The results were combined by weighting by the inverse of the square of the total error on each. Other methods of combining the muon and electron numbers gave the same result for $\Gamma_{b\bar{b}}/\Gamma_{had}$ within 0.3%. Errors on the combined measurement were derived by fluctuating the individual electron and muon results by each error in turn, taking into account whether errors are correlated or not between the two analyses. The lepton identification efficiencies, the conversion and hadronic background contributions, Monte Carlo statistical errors, the error due to simulation of radiation in the central detector volume (electrons), and the polar angle resolution error (muons) were assumed to be uncorrelated between the two channels. All other uncertainties, namely branching ratio, semileptonic decay modelling, and fragmentation errors, were treated as completely correlated between the two channels. This is a slightly conservative assumption for some error sources, since the two channels used different kinematic cuts. The combined errors are given in table 5. The combined result obtained was:

$$\frac{\Gamma_{b\bar{b}}}{\Gamma_{had}} = 0.220 \pm 0.002 \pm 0.006 \pm 0.011,$$

where the first error is statistical, the second arises from detector uncertainties and the third from b and c modelling and branching ratio uncertainties. The total error, including both statistical and systematic uncertainties, corresponds to $\pm 5.8\%$ of the measurement.

9 Conclusions

The fraction of hadronic Z^0 decays to $b\overline{b}$ pairs, $\Gamma_{b\bar{b}}/\Gamma_{had}$, has been measured from the yield of high momentum, high transverse momentum electrons and muons in hadronic Z^0 decay events. A value

$$\frac{\Gamma_{b\bar{b}}}{\Gamma_{had}} = 0.220 \pm 0.002 \pm 0.006 \pm 0.011$$

was obtained, where the first error is statistical, the second arises from detector performance uncertainties and the third from b and c quark modelling and branching ratio uncertainties. The measurement is completely limited by systematic errors. This result supersedes previous published OPAL measurements of $\Gamma_{b\bar{b}}$. Together with the OPAL measurement of the hadronic width of the Z^0, $\Gamma_{had} = 1738 \pm 12$ MeV [1], this result gives a value of

$$\Gamma_{b\bar{b}} = 382 \pm 22 \text{ MeV}.$$

The result is in good agreement with the Standard Model prediction for $\Gamma_{b\bar{b}}/\Gamma_{had}$. The ZFITTER program [22], with the latest OPAL Z^0 lineshape parameters [1], predicts $\Gamma_{b\bar{b}}/\Gamma_{had} = 0.217$ for a top quark mass of 150 GeV/c^2, a Higgs boson mass of 300 GeV/c^2, and $\alpha_s = 0.12$. Varying the top quark mass between 50 and 230 GeV/c^2 results in predictions varying between 0.219 and 0.213. The corresponding range for $\Gamma_{b\bar{b}}$ is 378–374 MeV, with a central prediction of 376 MeV.

The prospects for further reduction of the systematic errors on the measurement of $\Gamma_{b\bar{b}}$ using this approach are limited. With increasing data statistics, double-tag methods of measuring $\Gamma_{b\bar{b}}$, in which branching ratio, modelling, and fragmentation uncertainties largely cancel, will provide further improvements.

Acknowledgements

It is a pleasure to thank the SL Division for the efficient operation of the LEP accelerator, the precise information on the absolute energy, and their continuing close cooperation with our experimental group. In addition to the support staff at our own institutions we are pleased to acknowledge the
Department of Energy, USA,
National Science Foundation, USA,
Texas National Research Laboratory Commission, USA,
Science and Engineering Research Council, UK,
Natural Sciences and Engineering Research Council, Canada,
Fussefeld Foundation,
Israeli Ministry of Energy,
Israeli Ministry of Science,
Minerva Gesellschaft,
Japanese Ministry of Education, Science and Culture (the Monbusho) and a grant under the Monbusho International Science Research Program,
German Israeli Bi-national Science Foundation (GIF),
Direction des Sciences de la Matière du Commissariat à l'Energie Atomique, France,
Bundesministerium für Forschung und Technologie, FRG,
National Research Council of Canada, Canada,
A.P. Sloan Foundation and Junta Nacional de Investigação Científica e Tecnológica, Portugal.

References

[1] The LEP Collaborations, ALEPH, DELPHI, L3 and OPAL, Phys. Lett. **B276** (1992) 247;
OPAL Collaboration, P.D. Acton et al., *Precision Measurements of the Neutral Current from Hadron and Lepton Production at LEP*, to be published in Z. Phys. C., CERN-PPE/93-003.

[2] OPAL Collaboration, P.D. Acton et al., Z. Phys. **C55** (1992) 191.

[3] OPAL Collaboration, M.Z. Akrawy et al., Phys. Lett. **B263** (1991) 311.

[4] ALEPH Collaboration, D. Decamp et al., Phys. Lett. **B244** (1990) 551.

[5] DELPHI Collaboration, P. Abreu et al., Z. Phys. **C56** (1992) 47;
L3 Collaboration, B. Adeva et al., Phys. Lett. **B241** (1990) 416.

[6] DELPHI Collaboration, P. Abreu et al., Phys. Lett. **B281** (1992) 383;
MARK II Collaboration, J.F. Kral et al., Phys. Rev. Lett. **64** (1990) 1211;
MARK II Collaboration, R.G. Jacobsen et al., Phys. Rev. Lett. **67** (1991) 3347.

[7] L3 Collaboration, B. Adeva et al., Phys. Lett. **B261** (1991) 177.

[8] DELPHI Collaboration, P. Abreu et al., Phys. Lett. **B295** (1992) 383.

[9] See, for example,
J.H. Kühn, P.M. Zerwas, in: *Z Physics at LEP 1*, eds. G. Altarelli, R. Kleiss and C. Verzegnassi, Vol. 1 (CERN 89-08, 1989) pp.271–275.

[10] CLEO Collaboration, S. Henderson et al., Phys. Rev. **D45** (1992) 2212;
M. Worris, CLNS Thesis 91-05, Cornell University, 1991.

[11] OPAL Collaboration, K. Ahmet et al., Nucl. Instrum. Methods **A305** (1991) 275.

[12] M. Hauschild et al., Nucl. Instrum. Methods **A314** (1992) 74;
O. Biebel et al., Nucl. Instrum. Methods **A323** (1992) 169.

[13] OPAL Collaboration, G. Alexander et al., Z. Phys. **C52** (1991) 175.

[14] T. Sjöstrand, *PYTHIA 5.6 and JETSET 7.3: Physics and Manual*, CERN-TH.6488/92;
OPAL optimized parameters were used, as described in
OPAL Collaboration, M.Z. Akrawy et al., Z. Phys. **C47** (1990) 505.

[15] J. Allison et al., Nucl. Instrum. Methods **A317** (1992) 47.

[16] C. Peterson, D. Schlatter, I. Schmitt, P. Zerwas, Phys. Rev. **D27** (1983) 105.

[17] JADE Collaboration, W. Bartel et al., Z. Phys. **C33** (1986) 23;
JADE Collaboration, S. Bethke et al., Phys. Lett. **B213** (1988) 235.

[18] OPAL Collaboration, M.Z. Akrawy et al., Z. Phys. **C49** (1991) 375.

[19] OPAL Collaboration, G. Alexander et al., Phys. Lett. **B262** (1991) 341.

[20] ALEPH Collaboration, D. Decamp et al., Phys. Lett. **B266** (1991) 218.

[21] DELPHI Collaboration, P. Abreu et al., Phys. Lett. **B252** (1990) 140.

[22] D. Bardin et al., *ZFITTER: An Analytical Program for Fermion Pair Production in* e^+e^- *Annihilation*, CERN-TH 6443/92, May 1992.

[23] L3 Collaboration, B. Adeva et al., Phys. Lett. **B288** (1992) 412.

[24] G. Altarelli et al., Nucl. Phys. **B208** (1982) 365.

[25] N. Isgur, D. Scora, B. Grinstein, M.B. Wise, Phys. Rev. **D39** (1989) 799.

[26] DELCO Collaboration, W. Bacino et al., Phys. Rev. Lett. **43** (1979) 1073.

[27] CLEO Collaboration, D. Bortoletto et al., Phys. Rev. **D45** (1992) 21.

[28] D. Atwood and W.J. Marciano, Phys. Rev. **D41** (1990) 1736.

[29] ALEPH Collaboration, D. Buskulic et al., Phys. Lett. **B294** (1992) 145;
ALEPH Collaboration, D. Buskulic et al., *A Measurement of the b Baryon Lifetime*, submitted to Phys. Lett. B, CERN-PPE/92-138;
OPAL Collaboration, P.D. Acton et al., Phys. Lett. **B281** (1992) 394;
OPAL Collaboration, P.D. Acton et al., Phys. Lett. **B295** (1992) 357;
A preliminary OPAL measurement of $f(\mathrm{b} \to \Lambda_\mathrm{b}) B(\Lambda_\mathrm{b} \to \Lambda_\mathrm{c} \ell \nu X) = (1.5 \pm 0.35 \pm 0.26)\%$ derived using $B(\Lambda_\mathrm{c} \to \mathrm{pK}^- \pi^+)$=(4.3±1.0)% is taken from
X.C. Lou, XXVI International Conference on High Energy Physics (ICHEP 92), Dallas, 6–12 Aug 1992.

[30] See, for example,
R. Rückl, in: *Z Physics at LEP 1*, eds. G. Altarelli, R. Kleiss and C. Verzegnassi, Vol. 1 (CERN 89-08, 1989) pp. 311–317.

[31] Particle Data Group, K. Hikasa et al., Phys. Rev. **D45** (1992) 1.

[32] C. Quigg and J.L. Rosner, Phys. Rev. **D19** (1979) 1532.

[33] P. Heiliger and L.M. Sehgal, Phys. Lett. **B229** (1989) 409.

[34] ALEPH Collaboration, D. Buskulic et al., Phys. Lett. **B298** (1993) 479.

[35] L3 Collaboration, B. Adeva et al., Phys. Lett. **B259** (1991) 199;
L3 Collaboration, O. Adriani et al., Phys. Lett. **B286** (1992) 403.

Figure Captions

Figure 1: $N^{\sigma}_{\mathrm{d}E/\mathrm{d}x}$ distributions in four momentum bins for tracks in the 1991 data passing the other electron identification selection requirements. The fits to a Gaussian and a background histogram are superimposed. The background distribution is hatched.

Figure 2: Radius of reconstructed photon conversions (a) for 1990 data and (b) for 1991 data (points with error bars). The Monte Carlo distribution is superimposed (continuous line). The effect of the additional material introduced at small radii due to the installation of the microvertex detector in 1991 (inner beam pipe and two layers of silicon at radii 5.3 cm, 6.3 cm and 7.6 cm respectively) is evident, and is well modelled by the Monte Carlo simulation. The additional structure is due to the outer beam pipe at a radius of 8.0 cm and a carbon fibre tube at 23.5 cm separating the vertex and jet chamber.

Figure 3: (a) Distribution of the muon matching variable χ_{pos} for muon pairs produced by two-photon scattering processes $\mathrm{e^+e^-} \to \mathrm{e^+e^-}\mu^+\mu^-$, and for Z^0 decays to $\mu^+\mu^-$. (b) The χ_{pos} distribution for muon candidates in hadronic Z^0 decays for data and simulated events. The hatched histogram represents the prompt muons in simulated events.

Figure 4: Rest-frame momentum spectra for (a) $\mathrm{b} \to \mu$ (b) $\mathrm{b} \to \mathrm{c} \to \mu$ and (c) $\mathrm{c} \to \mu$ decays, for the models indicated. The effects of $\mathrm{b} \to \mathrm{u}\ell\nu$ decays (for (a) and (b)) and radiative corrections are included. The momentum spectra for electrons differ in the effects of radiative corrections. The momentum spectra of D mesons in B meson decays measured by CLEO was used in deriving the ACCMM and ISGW $\mathrm{b} \to \mathrm{c} \to \ell$ model spectra.

Figure 5: The (a) momentum and (b) p_t distributions for electron candidates passing all the selection cuts, after subtraction of hadronic and conversion background, and correction for the electron identification efficiency. The errors shown on the data points are statistical only—the statistical errors on the simulated events are not shown, but are comparable to those on the data. Since the electron background and efficiency corrections are not done bin-by-bin in the same bins as those shown here, these plots should be considered illustrative.

Figure 6: The (a) momentum and (b) p_t distributions for muon candidates passing all the selection cuts except that on p or p_t respectively. The positions of the p and p_t cuts are indicated by arrows. The errors shown on the data points are statistical only—the statistical errors on the simulated events are not shown, but are comparable to those on the data. There is also a $\pm 14\%$ error on the level of hadronic background.

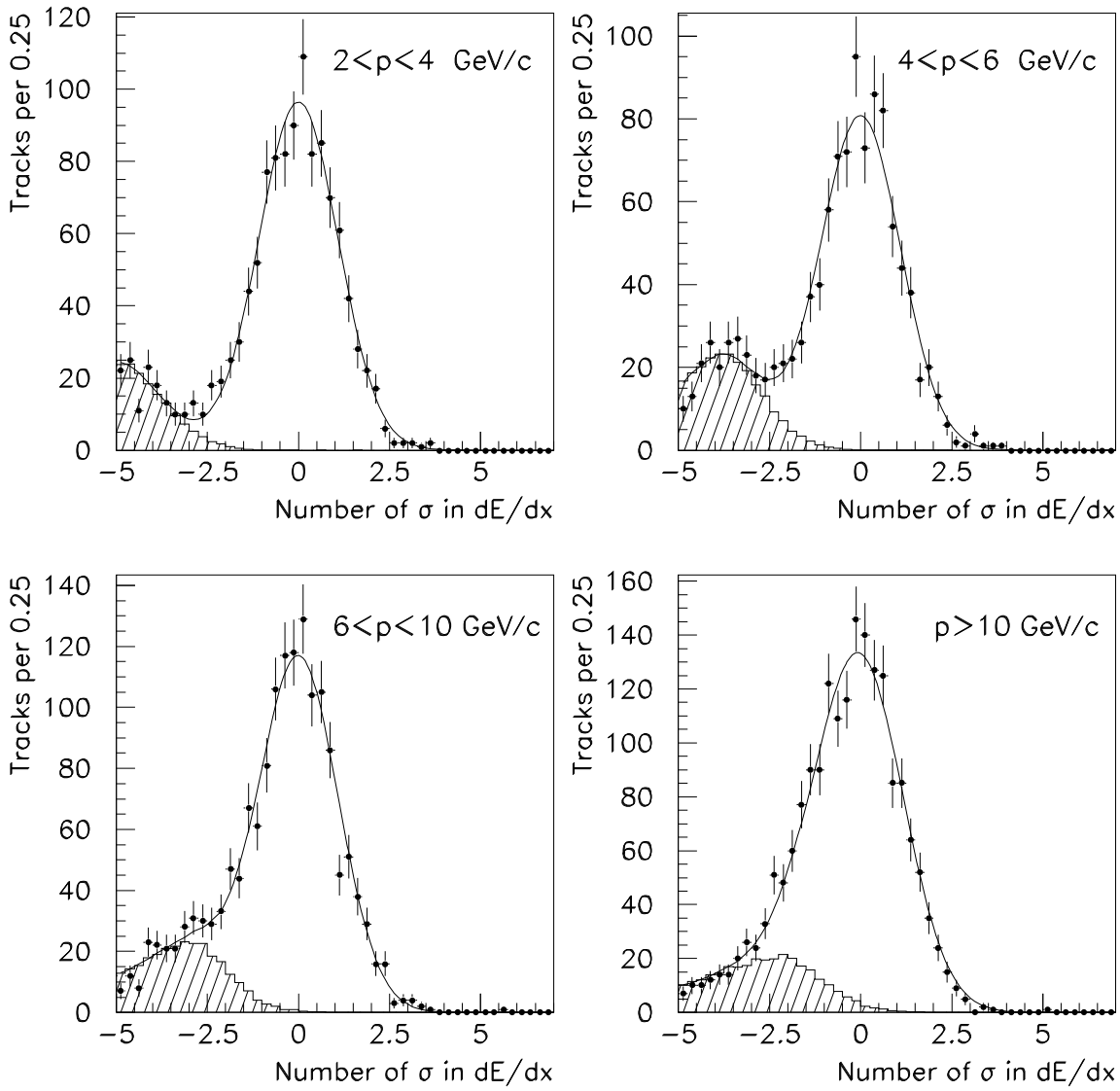
2<p<4 GeV/c
4<p<6 GeV/c
6<p<10 GeV/c
p>10 GeV/c
Tracks per 0.25
Number of σ in dE/dx

Figure 1

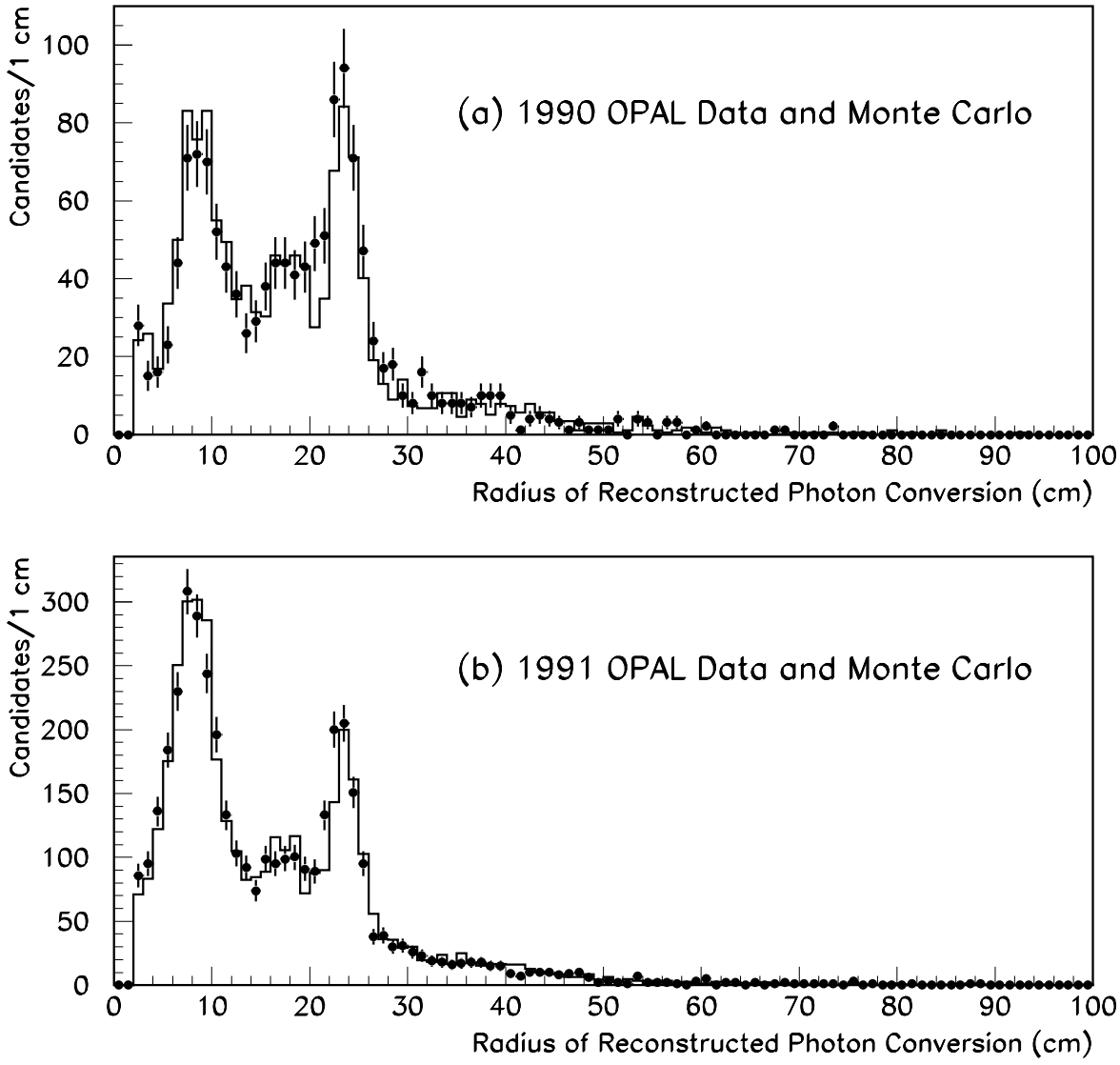
Candidates/1 cm
(a) 1990 OPAL Data and Monte Carlo
Radius of Reconstructed Photon Conversion (cm)
Candidates/1 cm
(b) 1991 OPAL Data and Monte Carlo
Radius of Reconstructed Photon Conversion (cm)

Figure 2

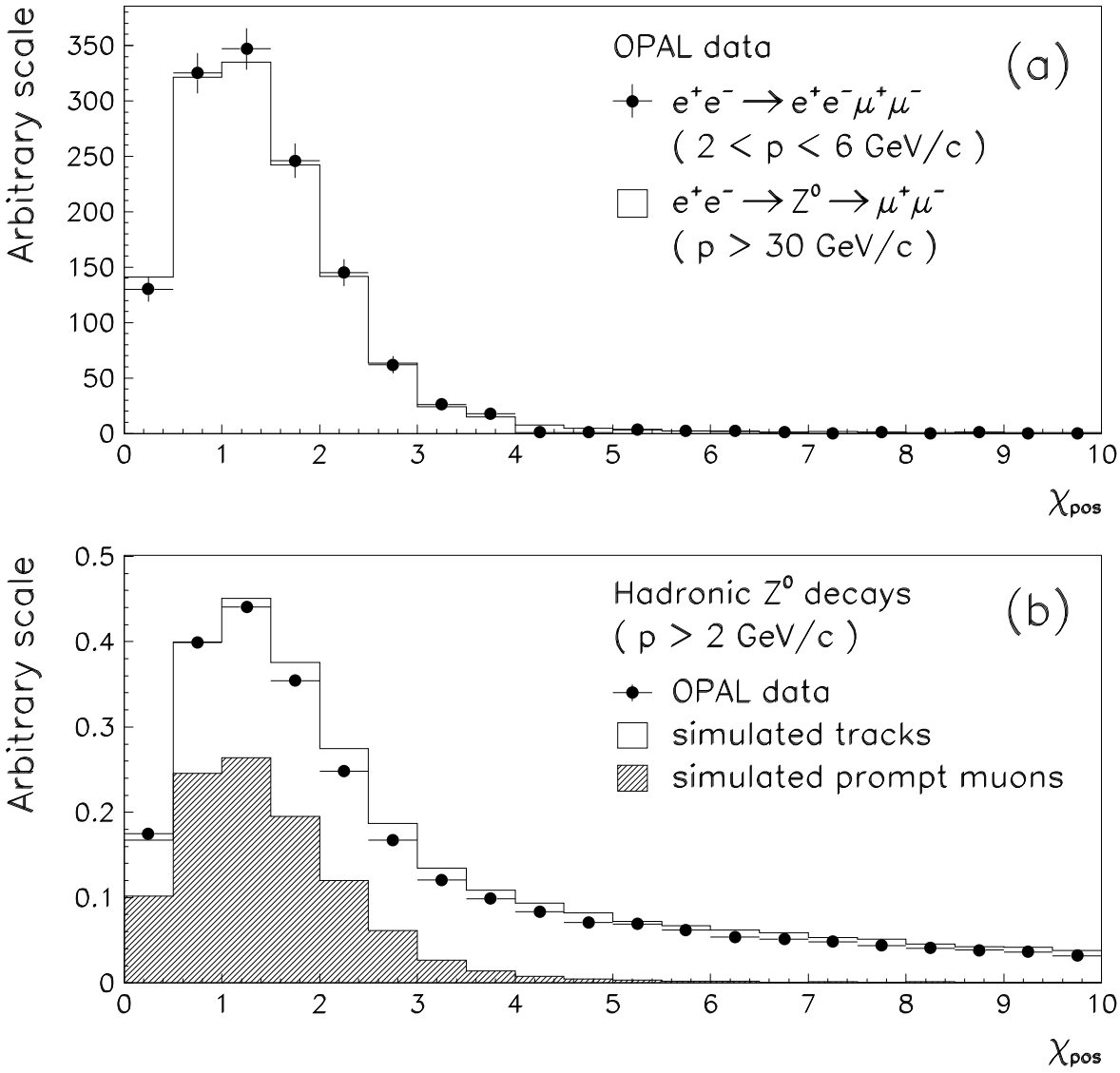
Arbitrary scale
OPAL data
(a)
$e^+e^- \rightarrow e^+e^-\mu^+\mu^-$
(2 < p < 6 GeV/c)
$e^+e^- \rightarrow Z^0 \rightarrow \mu^+\mu^-$
(p > 30 GeV/c)
χ_{pos}
Arbitrary scale
Hadronic Z^0 decays
(p > 2 GeV/c)
(b)
OPAL data
simulated tracks
simulated prompt muons
χ_{pos}

Figure 3

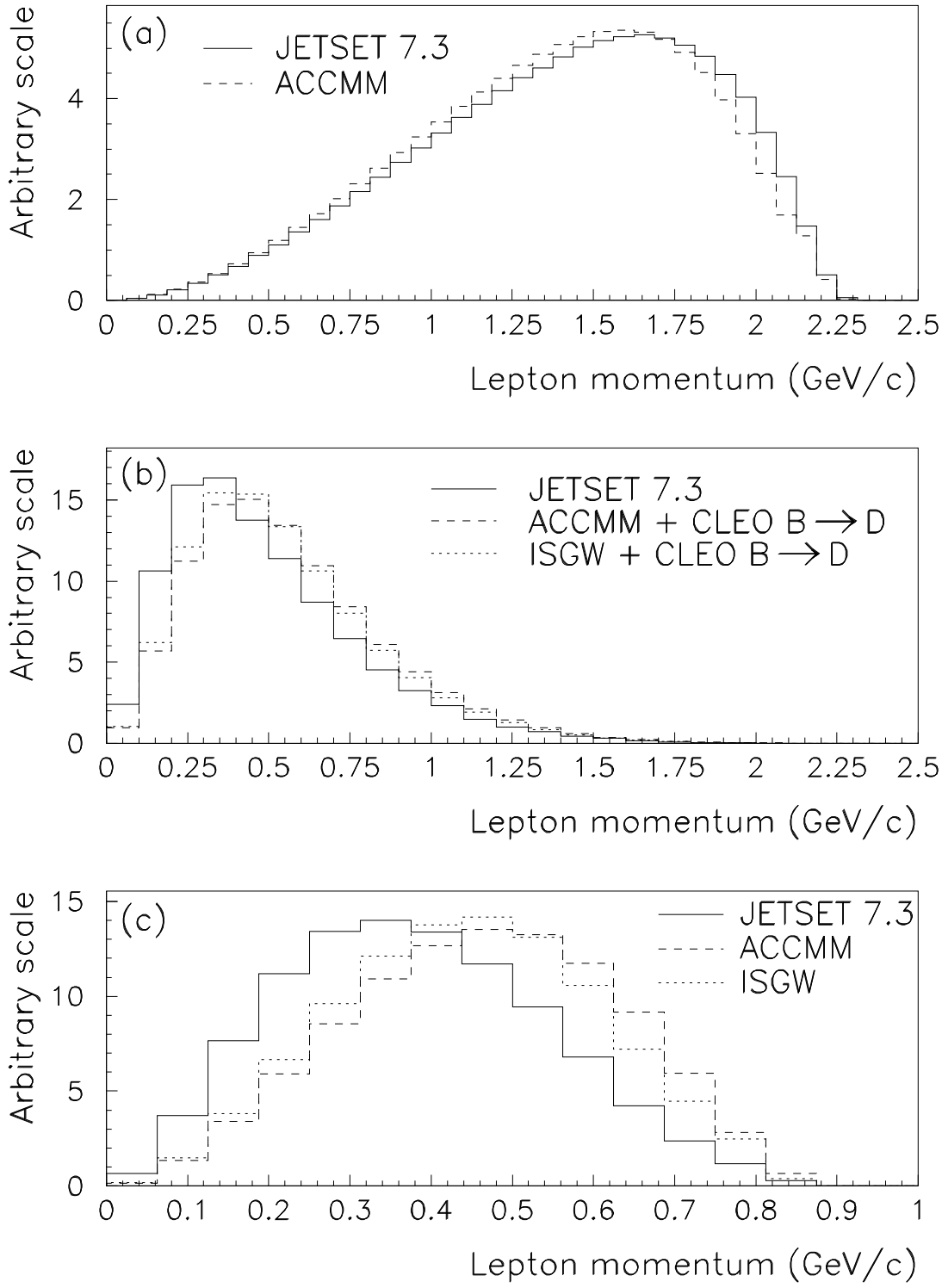
(a)
JETSET 7.3
ACCMM
Arbitrary scale
Lepton momentum (GeV/c)
(b)
JETSET 7.3
ACCMM + CLEO B → D
ISGW + CLEO B → D
Arbitrary scale
Lepton momentum (GeV/c)
(c)
JETSET 7.3
ACCMM
ISGW
Arbitrary scale
Lepton momentum (GeV/c)

Figure 4

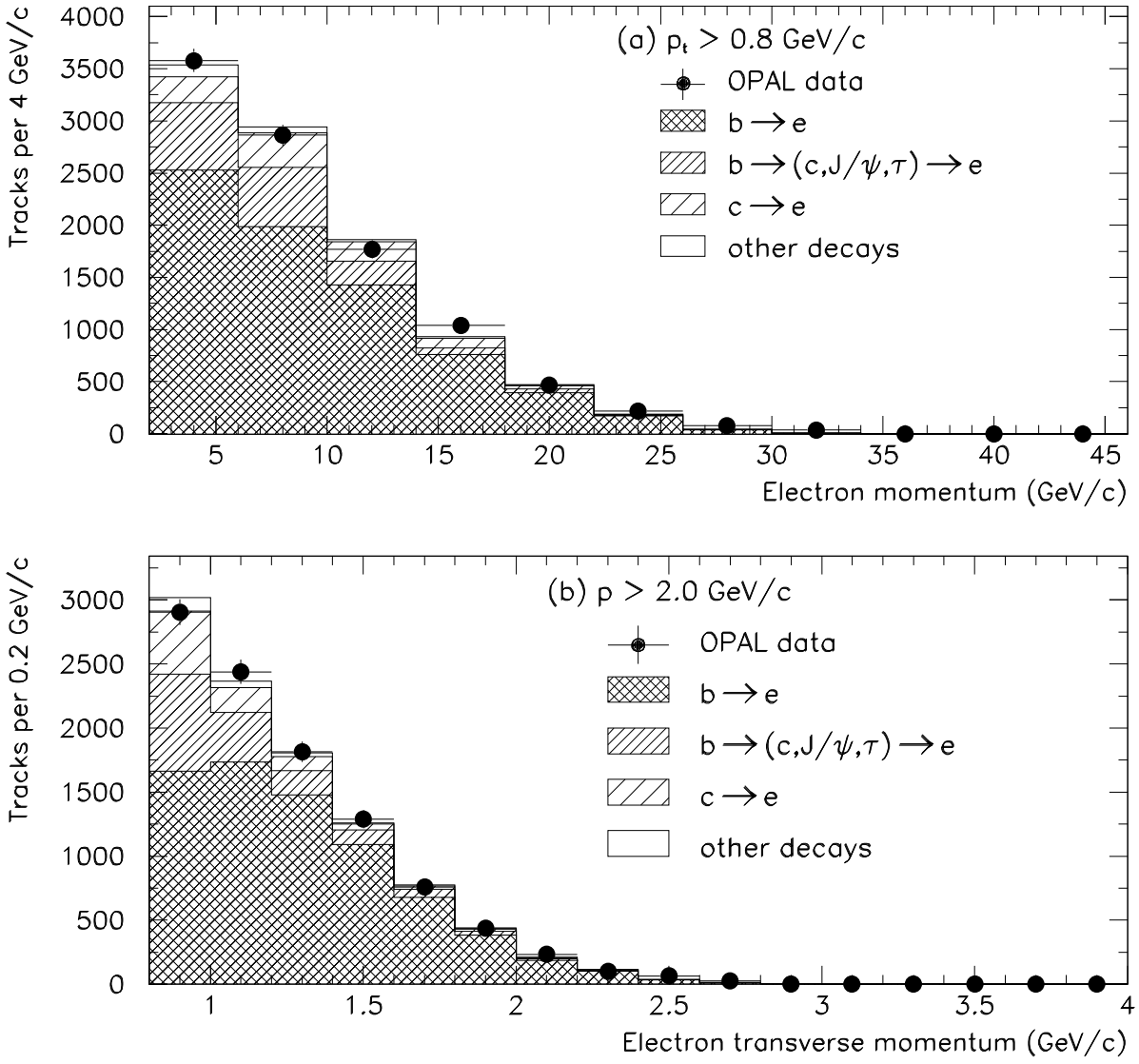
(a) p_t > 0.8 GeV/c
OPAL data
b → e
b → (c,J/ψ,τ) → e
c → e
other decays
Tracks per 4 GeV/c
Electron momentum (GeV/c)
(b) p > 2.0 GeV/c
OPAL data
b → e
b → (c,J/ψ,τ) → e
c → e
other decays
Tracks per 0.2 GeV/c
Electron transverse momentum (GeV/c)

Figure 5

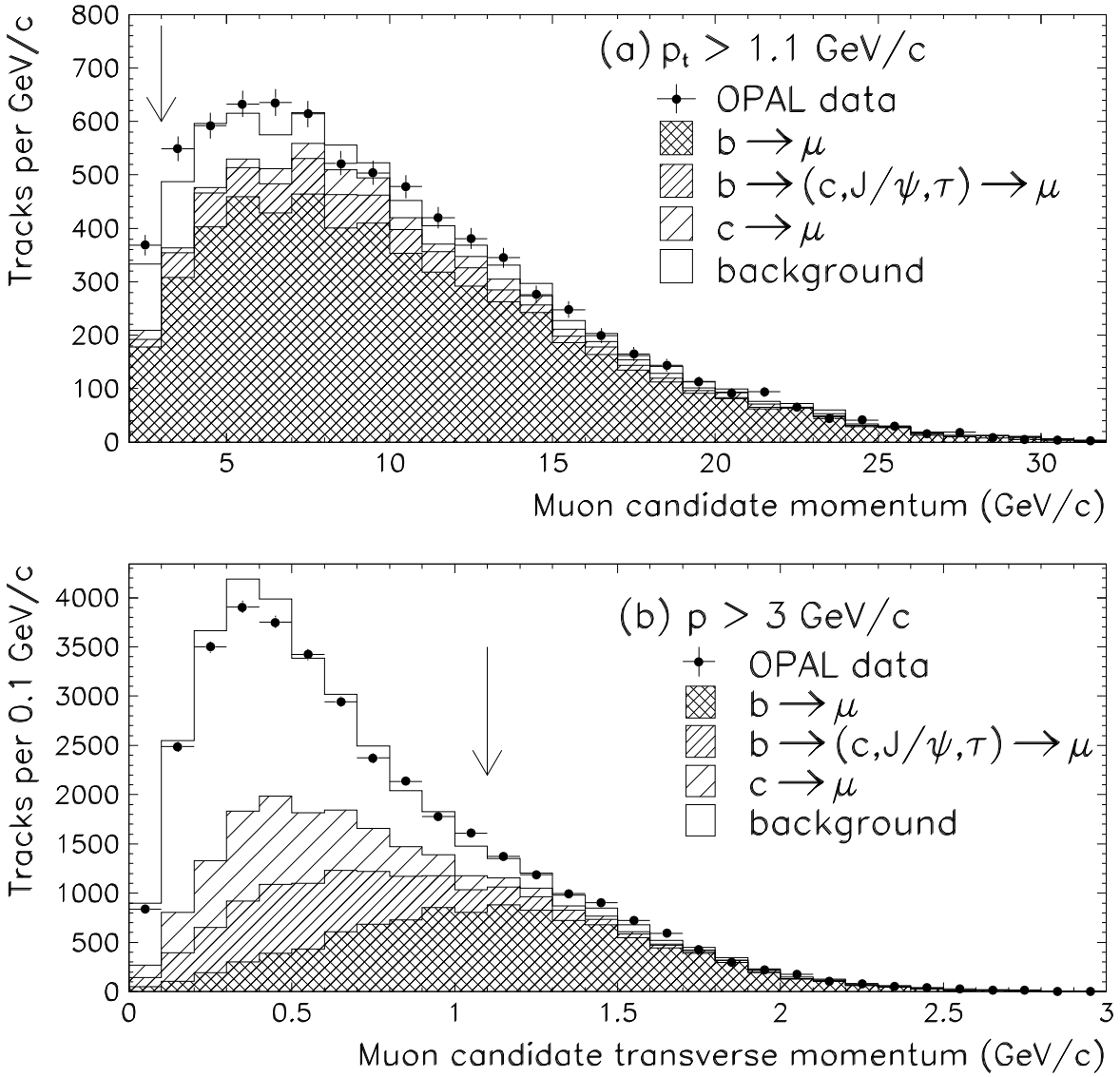
(a) p_t > 1.1 GeV/c
OPAL data
b → μ
b → (c,J/ψ,τ) → μ
c → μ
background
Tracks per GeV/c
Muon candidate momentum (GeV/c)
(b) p > 3 GeV/c
OPAL data
b → μ
b → (c,J/ψ,τ) → μ
c → μ
background
Tracks per 0.1 GeV/c
Muon candidate transverse momentum (GeV/c)

Figure 6